Testing the multipole structure and conservative dynamics of compact binaries using gravitational wave observations: The spinning case

Shilpa Kastha,[1,2,*] Anuradha Gupta,[3,†] K. G. Arun,[4,3,‡] B. S. Sathyaprakash,[3,5,6,§] and Chris Van Den Broeck[7,8,‖]

[1]*The Institute of Mathematical Sciences, C. I. T. Campus, Taramani, Chennai, 600113, India*
[2]*Homi Bhabha National Institute, Training School Complex, Anushakti Nagar, Mumbai, 400094, India*
[3]*Institute for Gravitation and the Cosmos, Department of Physics, Penn State University, University Park, Pennsylvania 16802, USA*
[4]*Chennai Mathematical Institute, Siruseri, 603103, India*
[5]*Department of Astronomy and Astrophysics, Penn State University, University Park, Pennsylvania 16802, USA*
[6]*School of Physics and Astronomy, Cardiff University, Cardiff, CF24 3AA, United Kingdom*
[7]*Nikhef - National Institute for Subatomic Physics, Science Park 105, 1098 XG Amsterdam, Netherlands*
[8]*Van Swinderen Institute for Particle Physics and Gravity, University of Groningen, Nijenborgh 4, 9747 AG Groningen, Netherlands*

(Received 17 May 2019; published 6 August 2019)

In an earlier work [S. Kastha *et al.*, Phys. Rev. D **98**, 124033 (2018)], we developed the *parametrized multipolar gravitational wave phasing formula* to test general relativity, for the nonspinning compact binaries in quasicircular orbit. In this paper, we extend the method and include the important effect of spins in the inspiral dynamics. Furthermore, we consider parametric scaling of post-Newtonian (PN) coefficients of the conserved energy for the compact binary, resulting in the parametrized phasing formula for nonprecessing spinning compact binaries in quasicircular orbit. We also compute the projected accuracies with which the second and third generation ground-based gravitational wave detector networks as well as the planned space-based detector LISA will be able to measure the multipole deformation parameters and the binding energy parameters. Based on different source configurations, we find that a network of third-generation detectors would have comparable ability to that of LISA in constraining the conservative and dissipative dynamics of the compact binary systems. This parametrized multipolar waveform would be extremely useful not only in deriving the first upper limits on any deviations of the multipole and the binding energy coefficients from general relativity using the gravitational wave detections, but also for science case studies of next generation gravitational wave detectors.

DOI: 10.1103/PhysRevD.100.044007

I. INTRODUCTION

Mergers of compact binaries are unique probes of the predictions of general relativity (GR) in the strong-gravity regime [1–5]. The gravitational wave (GW) detections made so far [6–12] by advanced LIGO [13] and advanced Virgo [14], have been used in various ways to test GR by employing different methods [8,9,15–18] to find very good agreement with the predictions of GR within the statistical uncertainties. With several more of such events expected to be detected in the future observing runs, developing efficient methods to carry out such tests will play a central role in extracting the best science from these observations. Ongoing developments of the science case for third-generation ground-based detectors such as Einstein Telescope [19] and Cosmic Explorer [20], and space-based LISA interferometer [21,22] further motivates developing generic methods to test GR using GWs.

There are a wide variety of tests proposed in the literature to assess GR using GW observations. These are often broadly classified as model independent tests (or theory-agnostic tests) and theory-dependent tests. Parametrized tests of GR [23–30], Parametrized post-Einsteinian framework [26,31], and inspiral-merger-ringdown consistency tests [32] are examples of the first kind whereas and the model dependent tests include tests aimed at looking for signatures of a specific alternative theory (or a class of alternative theories) such as those suggested in Refs. [33–36].

Recently, we proposed a new theory-agnostic test to probe the multipolar structure of compact binaries in GR [37]. The basic idea is to ask using GW observations how well we can infer the multipole structure of the gravitational

*shilpakastha@imsc.res.in
†axg645@psu.edu
‡kgarun@cmi.ac.in
§bss25@psu.edu
‖vdbroeck@nikhef.nl

field of the compact binary and search for potential deviations. In order to answer this question, we computed a parametrized gravitational waveform model explicitly keeping track of the contributions to the gravitational waveform from different radiative-multipole moments of the compact binary following the formalism developed in Refs. [38–43]. This prescription is built on the post-Newtonian (PN) approximation developed for compact binary systems with nonspinning component masses in quasicircular orbits. By introducing seven independent parameters associated to the deviation of the seven radiative-multipole moments from GR, we rederived the GW flux. This parametrized multipolar waveform facilitates tests of GR in a model independent way with GW observations [37]. We computed the projected accuracies on the measurements of these multipole coefficients for various ground-based and space-based detectors [37].

There is a strong astrophysical evidence that stellar mass black hole (BH) binaries [44,45] as well as supermassive BH binaries [46] may have highly spinning binary constituents. The spins of the compact binary components affect the binary dynamics and give rise to a very different radiation profile as compared to their nonspinning counterparts. Hence a physically realistic waveform model should account for the spin dynamics of compact binaries. Within the PN formalism, the gravitational waveform has been calculated considering the point masses with arbitrary spins up to a very high accuracy [47–73]. Hence, in this paper, we extend our parametrized multipolar GW energy flux as well as PN waveform model, presented in Ref. [37], with spin-orbit and spin-spin contributions from binary components. We assume that the component spins are either aligned or antialigned with respect to the orbital angular momentum of the binary which is inspiraling in quasicircular orbit. Here, in addition to the multipolar structure, we present the phasing formula which also parametrizes the conservative dynamics of the binary. This is achieved by introducing free parameters at each PN order in the binding energy expression which take value unity in GR, by definition.

Having included the effects of spins in our parametrized test of multipole structure, we use the Fisher information matrix based parameter estimation scheme to compute projected bounds on the various multipolar parameters. Along with the complete study on the bounds of the multipolar parameters, we also provide the bounds on the parameters associated to conservative sector for the first time in this paper. We consider GW observation through networks of the various second and third generation ground-based detectors as well the proposed space-based LISA mission [22]. Inclusion of spin effects not only increases the dimensionality of the parameter space but also degrades the measurement accuracy of parameters. We find that a network of third-generation ground-based detectors and the space-based LISA mission would have comparable sensitivity to detect potential deviations in the multipolar structure of compact binaries.

This paper is organized as follows. In Sec. II we discuss our computational scheme for the multipolar parametrized gravitational wave energy flux. In Sec. III we explore the modifications in the parametrized frequency domain (TaylorF2) waveform due to the various contributions from spins. Thereafter, in Sec. IV we briefly describe the parameter estimation techniques we use in this paper. Section V provides a detailed description about the various GW detector configurations used for our analysis. In Sec. VI we discuss the bounds on the multipole coefficients for various GW detectors and Sec. VII presents our concluding remarks.

II. PARAMETRIZED GRAVITATIONAL WAVE ENERGY FLUX

During the inspiral phase of the compact binary dynamics, the radiation reaction time scale is much longer than the timescale for orbital motion. Due to this separation of timescales, two vital ingredients for computing the phase evolution are the *conserved orbital energy* of the binary and the *gravitational wave energy flux* from the system. While the former characterizes the conservative dynamics of the binary, the latter describes the dissipative dynamics.

The computation of the multipolar parametrized flux formula makes use of the entire machinery of the multipolar post-Minkowskian and post-Newtonian formalism developed over past several years [39,42,43,52,74–78] (see [79] for a review.) Following Ref. [37], we use the GW energy flux parametrized in terms of the various radiative multipole moments of compact binary while including contributions from the spins of the binary components in quasicircular orbits. More explicitly, to capture the generic deviations from GR, parametric deviations are introduced at the level of mass-type (U_L) and current-type (V_L) radiative multipole moments through simple scaling relationships of the kind

$$U_L \to \mu_l U_L^{\rm GR}, \tag{2.1}$$

$$V_L \to \epsilon_l V_L^{\rm GR}, \tag{2.2}$$

where $\mu_l = 1 + \delta U_L/U_L^{\rm GR}$ and $\epsilon_l = 1 + \delta V_L/V_L^{\rm GR}$ take the value unity in GR. The conservative dynamics of the binary also gets imprinted on the GW phasing formula via the PN expression for conserved energy. If the underlying theory of gravity is not GR, the corresponding PN coefficients could be different. In our framework, these are parametrized by a set of parameters $\{\alpha_k\}$ which are all unity in GR.

A modifed theory of gravity could predict one or more of these multipole moments to be different from that of GR. It may also predict the conserved energy of the binary to be different from GR. In our formalism the set of parameters $\{\mu_l, \epsilon_l, \alpha_k\}$ parametrize all such differences. Hence a measurement of these coefficients would give us a direct handle on possible deviations of the multipole moments and/or conservative dynamics from the GR predictions. Indeed, it is possible that these coefficients may be

functions of the binary parameters (masses, spins etc.) in a modified theory. However, since we have no prior knowledge about the "true" underlying theory of gravity, any method to look for its signatures has to be theory-agnostic which motivates our parametrization. (A more generic parametrization may involve introducing free parameters at every PN order of all the multipole moments. Obviously, given the large number of free parameters, this would result in bounds which are uninformative.)

In this paper we focus on the contributions to the flux from spin angular momentum of the binary components and hence quote only the spin-dependent part of the parametrized GW energy flux which may be added to the nonspinning results of [37] to get the complete phasing. Among the few different approaches to consider the PN spin corrections to the conservative dynamics as well as gravitational radiation from a compact binary system, we adopt the PN iteration scheme in harmonic coordinates [58] to obtain spin contributions to the radiative moments in GR which we further rescale as described in Eqs. (2.1)–(2.2).

We closely follow the prescription given in Refs. [52,54,56–58] to account for the contributions to the conservative and dissipative sectors of the compact binary dynamics from the individual spins. In our notation, the individual spins of the component masses, m_1 and m_2 are $\mathbf{S_1}$ and $\mathbf{S_2}$ with quadrupolar polarizabilities κ_1 and κ_2, respectively, which are unity for Kerr black holes. We denote the total mass for the system to be $m = m_1 + m_2$, relative mass difference, $\delta = (m_1 - m_2)/m$ and the symmetric mass ratio, $\nu = m_1 m_2/m^2$. Furthermore following the usual notation, we present our results in terms of the symmetric combination of the quadrupolar polarizabilities, $\kappa_+ = \kappa_1 + \kappa_2$ and the antisymmetric combination, $\kappa_- = \kappa_1 - \kappa_2$. Our results are expressed in the center of mass frame where the spin variables $\mathbf{S}$ and $\mathbf{\Sigma}$ have the following relations with the spins of each of the constituent masses of the binary,

$$\mathbf{S} = \mathbf{S_1} + \mathbf{S_2}, \tag{2.3}$$

$$\mathbf{\Sigma} = m\left(\frac{\mathbf{S_2}}{m_2} - \frac{\mathbf{S_1}}{m_1}\right), \tag{2.4}$$

and $S_L = \mathbf{S}\cdot\hat{\mathbf{L}}$ and $\Sigma_L = \mathbf{\Sigma}\cdot\hat{\mathbf{L}}$ are the projections along the direction (with $\hat{\mathbf{L}} = \mathbf{L}/|\mathbf{L}|$) of orbital angular momentum ($\mathbf{L}$).

Depending on the order of spin corrections, the GW flux schematically has the following structure,

$$\mathcal{F} = \mathcal{F}_{\rm NS} + \mathcal{F}_{\rm SO} + \mathcal{F}_{\rm SS} + \mathcal{F}_{\rm SSS} + \cdots, \tag{2.5}$$

where $\mathcal{F}_{\rm NS}$ is the nonspinning contribution computed in Eq. (2.8) of Ref. [37], $\mathcal{F}_{\rm SO}$ is the spin-orbit (SO) contribution which linearly depends on the spins, and $\mathcal{F}_{\rm SS}$ is quadratic in spins arising due to the spin-spin (SS) interactions. Similarly $\mathcal{F}_{\rm SSS}$ denotes the cubic-in-spin effects on the GW energy flux. Here we report the parametrized multipolar flux accounting for spin-orbit effects up to 3.5PN order and quandratic-in-spin contributions up to 3PN order. We do not provide the cubic spin and the partial quadratic-in-spin contribution at 3.5PN order. The nonspinning flux computed in Ref. [37] should be added to these to obtain the total flux. We provide explicit expressions for the spin-orbit and quadratic-in-spin contributions to multipolar parametrized GW fluxes in the following subsections.

A. Spin-orbit contribution

Considering the leading order spin corrections to the multipole moments as well as in the equation of motion (EOM) and following the same technique as prescribed in Refs. [52,54,56], we recompute the parametrized SO part of the energy flux, which is given as

$$\begin{aligned}
\mathcal{F}_{\rm SO} = \frac{32}{5}\frac{c^5}{G}\nu^2\mu_2^2 x^5\Bigg\{&\frac{x^{3/2}}{Gm^2}\left(-4S_L + \delta\Sigma_L\left[-\frac{4}{3}+\frac{\hat{\epsilon}_2^2}{12}\right]\right) + \frac{x^{5/2}}{Gm^2}\left(S_L\left[\frac{316}{63}-\frac{514}{63}\nu - \hat{\mu}_3^2\left(\frac{598}{63}-\frac{2392}{63}\nu\right) - \hat{\epsilon}_2^2\left(\frac{43}{126}-\frac{86}{63}\nu\right)\right.\right.\\
&\left.\left. + \hat{\epsilon}_3^2\left(\frac{20}{63}-\frac{20}{21}\nu\right)\right] + \delta\Sigma_L\left[\frac{208}{63}-\frac{10}{9}\nu - \hat{\mu}_3^2\left(\frac{1025}{252}-\frac{1025}{84}\nu\right) - \hat{\epsilon}_2^2\left(\frac{367}{1008}-\frac{11}{18}\nu\right) + \hat{\epsilon}_3^2\left(\frac{20}{63}-\frac{20}{21}\nu\right)\right]\right)\\
&+ \frac{\pi x^3}{Gm^2}\left(-16S_L + \delta\Sigma_L\left[-\frac{16}{3}+\frac{\hat{\epsilon}_2^2}{6}\right]\right) + \frac{x^{7/2}}{Gm^2}\left(S_L\left[\frac{58468}{1323}+\frac{154424}{1323}\nu+\frac{3494}{1323}\nu^2 + \hat{\mu}_3^2\left(\frac{120121\nu^2}{1134}-\frac{345665\nu}{1512}+\frac{65491}{1296}\right)\right.\right.\\
&+ \hat{\mu}_4^2\left(-\frac{272392\nu^2}{1323}+\frac{544784\nu}{3969}-\frac{272392}{11907}\right) + \hat{\epsilon}_2^2\left(-\frac{1534\nu^2}{3969}-\frac{1165\nu}{2646}+\frac{2131}{15876}\right) + \hat{\epsilon}_3^2\left(-\frac{7300\nu^2}{567}+\frac{7150\nu}{567}-\frac{1556}{567}\right)\\
&\left. + \hat{\epsilon}_4^2\left(\frac{5741\nu^2}{882}-\frac{5741\nu}{1176}+\frac{5741}{7056}\right)\right] + \delta\Sigma_L\left[\frac{28423\nu^2}{3969}+\frac{366697\nu}{7938}+\frac{49844}{3969} + \hat{\mu}_3^2\left(\frac{319661\nu^2}{18144}-\frac{811795\nu}{9072}+\frac{253385}{9072}\right)\right.\\
&+ \hat{\mu}_4^2\left(-\frac{3184\nu^2}{49}+\frac{7960\nu}{147}-\frac{1592}{147}\right) + \hat{\epsilon}_2^2\left(-\frac{41471\nu^2}{127008}-\frac{37585\nu}{31752}+\frac{14383}{63504}\right) + \hat{\epsilon}_3^2\left(-\frac{490\nu^2}{81}+\frac{5140\nu}{567}-\frac{188}{81}\right)\\
&\left.\left. + \hat{\epsilon}_4^2\left(\frac{5741}{7056}-\frac{28705}{7056}\nu+\frac{5741}{1176}\nu^2\right)\right]\right)\Bigg\}.
\end{aligned} \tag{2.6}$$

Spin-orbit corrections to the flux first appear at 1.5PN order due to spin-dependent terms in mass quadrupole moments at 1.5PN order and current quadrupole moment at 0.5PN order. Hence the leading order SO corrections bring in the μ_2 and ϵ_2 in the parametrized GW flux at 1.5PN. As clearly stated in Ref. [52], at 2.5PN order the SO contributions come from mass- and current-type quadrupole and octupole moments, which is evident from Eq. (2.6) since only μ_2, μ_3, ϵ_2, and ϵ_3 are present up to 2.5PN order. At 3PN order, the spin dependences come from the 1.5PN tail integral performed on mass quadrupole moment and the 2.5PN tail integral performed on current quadrupole moment [54]. Hence at 3PN order only μ_2 and ϵ_2 are present. As we go to higher order we find that at 3.5PN order, μ_4 and ϵ_4 are also present along with the lower order coefficients. As a check on the calculation, in the limit $\mu_2=\mu_3=\mu_4=\mu_5=\epsilon_2=\epsilon_3=\epsilon_4=1$, Eq. (2.6) reduces to Eq. (4) of Ref. [52].

B. Spin-spin contribution

Quadratic-in-spin corrections first appear at 2PN order to the GW flux and the waveform (see Refs. [47,49,51,66,80] for details), whereas SS terms at 3PN are first calculated in Ref. [57].

Along with the terms quadratic-in-spin in the EOM, the complete SS contributions to the flux are generated from the four leading multipole moments, I_{ij}, I_{ijk}, J_{ij}, and J_{ijk}. Hence $\mathcal{F}_{\rm SS}$ is completely parametrized by μ_2, μ_3, ϵ_2, and ϵ_3 [see Eq. (2.7)]. We have also written the SS contribution at 3.5PN order arising from the two leading order tail integrals performed on mass and current quadrupole moments. However, at 3.5PN order SS contributions are partial. Hence these contributions will be neglected for the waveform computations.

$$
\begin{aligned}
\mathcal{F}_{\rm SS}=&\frac{32}{5}\frac{c^5}{G}\nu^2\mu_2^2x^5\frac{1}{G^2m^4}\Bigg\{x^2\left(S_L^2[4+2\kappa_+]+S_L\Sigma_L[2\kappa_+\delta+4\delta-2\kappa_-]+\Sigma_L^2\left[\frac{\hat{\epsilon}_2^2}{16}+\kappa_+-\delta\kappa_--(4+2\kappa_+)\nu\right]\right)\\
&+x^3\Bigg(S_L^2\left[-\frac{1198}{63}-\frac{46\kappa_+}{7}+\frac{55\delta\kappa_-}{21}+\hat{\mu}_3^2\left(\frac{1367}{168}+\frac{1367\kappa_+}{336}-\frac{\delta\kappa_-}{1008}\right)+\hat{\epsilon}_2^2\left(\frac{1}{6}+\frac{\kappa_+}{12}-\frac{\delta\kappa_-}{18}\right)+\frac{20}{63}\hat{\epsilon}_3^2\right.\\
&\left.+\nu\left(\frac{82}{7}+\frac{41\kappa_+}{7}-\hat{\mu}_3^2\left[\frac{1367}{42}+\frac{1367\kappa_+}{84}\right]-\hat{\epsilon}_2^2\left[\frac{2}{3}+\frac{\kappa_+}{3}\right]\right)\right]+S_L\Sigma_L\left[-\frac{193\delta\kappa_+}{21}-\frac{1436\delta}{63}+\frac{193\kappa_-}{21}\right.\\
&+\hat{\mu}_3^2\left(\frac{293\delta\kappa_+}{72}+\frac{1367\delta}{168}-\frac{293\kappa_-}{72}\right)+\hat{\epsilon}_2^2\left(\frac{5\delta\kappa_+}{36}-\frac{143\delta}{252}-\frac{5\kappa_-}{36}\right)+\frac{40}{63}\delta\hat{\epsilon}_3^2+\nu\left(\frac{41\delta\kappa_+}{7}+\frac{82\delta}{7}-\frac{49\kappa_-}{3}\right.\\
&\left.\left.+\hat{\mu}_3^2\left[\frac{293\kappa_-}{18}-\frac{1367\delta}{42}-\frac{1367\kappa_+\delta}{84}\right]-\hat{\epsilon}_2^2\left[\frac{\delta\kappa_+}{3}+\frac{2\delta}{3}-\frac{5\kappa_-}{9}\right]\right)\right]+\Sigma_L^2\left[-\frac{26}{9}-\frac{193\kappa_+}{42}+\frac{193\delta\kappa_-}{42}+\hat{\mu}_3^2\left(\frac{293\kappa_+}{144}-\frac{293\delta\kappa_-}{144}\right)\right.\\
&-\hat{\epsilon}_2^2\left[\frac{31}{56}-\frac{5\kappa_+}{72}+\frac{5\delta\kappa_-}{72}\right]+\frac{20}{63}\hat{\epsilon}_3^2+\nu\left(\frac{1562}{63}+\frac{619\kappa_+}{42}-\frac{233\delta\kappa_-}{42}-\hat{\mu}_3^2\left[\frac{1367}{168}+\frac{12305\kappa_+}{1008}-\frac{8203\delta\kappa_-}{1008}\right]\right.\\
&\left.\left.+\hat{\epsilon}_2^2\left(\frac{167}{168}-\frac{13\kappa_+}{36}+\frac{2\delta\kappa_-}{9}\right)-\frac{80}{63}\hat{\epsilon}_3^2\right)+\nu^2\left(-\frac{41\kappa_+}{7}-\frac{82}{7}+\hat{\mu}_3^2\left[\frac{1367}{42}+\frac{1367\kappa_+}{84}\right]+\hat{\epsilon}_2^2\left[\frac{2}{3}+\frac{\kappa_+}{3}\right]\right)\right]\Bigg)\\
&+\pi x^{7/2}\left(S_L^2[16+8\kappa_+]+S_L\Sigma_L[8\kappa_+\delta+16\delta-8\kappa_-]+\Sigma_L^2\left[\frac{\hat{\epsilon}_2^2}{8}+4\kappa_+-4\delta\kappa_--(16+8\kappa_+)\nu\right]\right)\Bigg\}. \qquad (2.7)
\end{aligned}
$$

As an algebraic check, in the limit, $\mu_2=\mu_3=\mu_4=\mu_5=\epsilon_2=\epsilon_3=\epsilon_4=1$ for Eq. (2.7), we confirm the recovery of the accurate expression for SS contribution to GW flux in GR reported in Eq. (4.14) of Ref. [57].

III. PARAMETRIZED MULTIPOLAR GRAVITATIONAL WAVE PHASING

The GW phase and its frequency evolution are obtained by using the energy conservation law which essentially balances the rate of change of conserved orbital energy E and the emitted GW flux,

$$\mathcal{F}=-\frac{d}{dt}E. \qquad (3.1)$$

Hence an accurate model for conserved orbital energy is needed to obtain the GW phasing formula.

In GR, for a nonspinning compact binary inspiraling in quasicircular orbit, the expression for the conserved energy per unit mass is given in Refs. [78,81–86], whereas the SO corrections up to 3.5PN order and the SS corrections up to 3PN order are quoted in Refs. [52,54,56,57].

In alternative theories of gravity, along with the deformations at the level of multipole moments, we expect the conserved orbital energy to be deformed as well. In order to

incorporate theses effects, we introduce free parameters α_k, characterizing the deviations at different PN orders in the expression of conserved energy defined in GR for compact binaries in aligned (or antialigned)-spin configuration. For spin corrections to conservative dynamics we consider SO contributions upto 3.5PN order and SS contributions at 3PN order to the energy. The 3.5PN closed-form expression for the parametrized conserved energy reads as

$$
\begin{aligned}
E(v) = -\frac{1}{2}\nu\alpha_0 v^2\Bigg[1 &- \left(\frac{3}{4}+\frac{1}{12}\nu\right)\hat{\alpha}_2 v^2 + \left\{\frac{14}{3}S_L + 2\delta\Sigma_L\right\}\frac{\hat{\alpha}_3}{Gm^2}v^3 \\
&- \left\{\frac{27}{8} - \frac{19}{8}\nu + \frac{1}{24}\nu^2 + \frac{S_L^2}{G^2m^4}(\kappa_+ + 2) + \frac{S_L\Sigma_L}{G^2m^4}(\delta\kappa_+ + 2\delta - \kappa_-) + \frac{\Sigma_L^2}{G^2m^4}\left(\frac{1}{2}\kappa_+ - \frac{\delta}{2}\kappa_- - \nu[\kappa_+ + 2]\right)\right\}\hat{\alpha}_4 v^4 \\
&+ \left\{\left[11 - \frac{61}{9}\nu\right]S_L + \left[3 - \frac{10}{3}\nu\right]\delta\Sigma_L\right\}\frac{\hat{\alpha}_5}{Gm^2}v^5 \\
&- \left\{\frac{675}{64} - \left(\frac{34445}{576} - \frac{205}{96}\pi^2\right)\nu + \frac{155}{96}\nu^2 + \frac{35}{5184}\nu^3 + \frac{S_L^2}{G^2m^4}\left(\left[\frac{5}{3}\delta\kappa_- + \frac{25}{6}\kappa_+ - \frac{50}{9}\right] - \nu\left[\frac{5}{6}\kappa_+ + \frac{5}{3}\right]\right)\right. \\
&+ \frac{S_L\Sigma_L}{G^2m^4}\left(\left[\frac{5}{2}\delta\kappa_+ - \frac{25}{3}\delta - \frac{5}{2}\kappa_-\right] - \nu\left[\frac{5}{6}\delta\kappa_+ + \frac{5}{3}\delta + \frac{35}{6}\kappa_-\right]\right) \\
&\left.+ \frac{\Sigma_L^2}{G^2m^4}\left(\left[\frac{5}{4}\kappa_+ - \frac{5}{4}\delta\kappa_- - 5\right] - \nu\left[\frac{5}{4}\kappa_+ + \frac{5}{4}\delta\kappa_- - 10\right] + \nu^2\left[\frac{5}{6}\kappa_+ + \frac{5}{3}\right]\right)\right\}\hat{\alpha}_6 v^6 \\
&+ \left\{\left(\frac{135}{4} - \frac{367}{4}\nu + \frac{29}{12}\nu^2\right)S_L + \left(\frac{27}{4} - 39\nu + \frac{5}{4}\nu^2\right)\delta\Sigma_L\right\}\frac{\hat{\alpha}_7}{Gm^2}v^7\Bigg],
\end{aligned}
\tag{3.2}
$$

with $\hat{\alpha}_i = \alpha_i/\alpha_0$. To obtain the gravitational waveform in frequency domain under the stationary phase approximation [87], we use the standard prescription outlined in Refs. [88,89]. The important difference here is that we use the parametrized expressions for the GW flux and conserved energy given by Eq. (2.5) and (3.2) respectively. Further we consider the amplitude to be at the leading quadrupolar order. The standard *restricted* PN waveform in frequency domain, thus, reads as

$$\tilde{h}_S(f) = \mathcal{A}\mu_2 f^{-7/6} e^{i\psi_S(f)}, \tag{3.3}$$

with $\mathcal{A}=\mathcal{M}_c^{5/6}/\sqrt{30}\pi^{2/3}D_L; \mathcal{M}_c=(m_1m_2)^{3/5}/(m_1+m_2)^{1/5}$ and D_L are the chirp mass and luminosity distance. In the case of LISA, to account for its triangular geometry, we multiply the gravitational waveform by a factor of $\sqrt{3}/2$ while calculating the Fisher matrix for LISA [90]. The parametrized multipolar phasing, $\psi_S(f)$, has the same structure as that of the energy flux [see Eq. (2.5)]. Schematically the parametrized phasing formula can be written as,

$$
\begin{aligned}
\psi_S(f) = 2\pi f t_c - \phi_c - \frac{\pi}{4} \\
+ \frac{3\alpha_0}{128\nu v^5\mu_2^2}[\psi_{\rm NS}(f) + \psi_{\rm SO}(f) + \psi_{\rm SS}(f)],
\end{aligned}
\tag{3.4}
$$

where the parametrized nonspinning part, $\psi_{\rm NS}(f)$ is given by Eq. (A.2) in Ref. [37]. Here we show only the SO and SS parts: $\psi_{\rm SO}(f)$ and $\psi_{\rm SS}(f)$. As mentioned earlier, we do not account for the partial contribution due to the spin-spin interactions to the phasing formula at the 3.5PN order.

To evaluate the parametrized TaylorF2 phasing for aligned spin binaries, we use the conventional notations for the spin variables $(\boldsymbol{\chi_1},\boldsymbol{\chi_2})$, with the following redefinitions,

$$\boldsymbol{\chi_1} = Gm_1^2\mathbf{S}_1, \tag{3.5}$$

$$\boldsymbol{\chi_2} = Gm_2^2\mathbf{S}_2. \tag{3.6}$$

Furthermore, we use $\chi_s = (\chi_1+\chi_2)/2$ and $\chi_a = (\chi_1-\chi_2)/2$ to present the phasing formula, where χ_1 and χ_2 are the projections of $\boldsymbol{\chi_1}$ and $\boldsymbol{\chi_2}$ along the orbital angular momentum, respectively. These spin variables have the following relations,

$$S_L = Gm^2[\delta\chi_a + (1-2\nu)\chi_s], \tag{3.7}$$

$$\Sigma_L = -Gm^2[\delta\chi_s + \chi_a]. \tag{3.8}$$

Finally we write down the expressions for $\psi_{\rm SO}$ and $\psi_{\rm SS}$, the main results of this paper, below

$$
\begin{aligned}
\psi_{\rm SO} = {} & v^3\left\{\left[\frac{32}{3}+\frac{80}{3}\hat{\alpha}_3+\frac{1}{3}\hat{\epsilon}_2^2-\left(\frac{32}{3}+\frac{40}{3}\hat{\alpha}_3+\frac{4}{3}\hat{\epsilon}_2^2\right)\nu\right]\chi_s+\left[\frac{32}{3}+\frac{80}{3}\hat{\alpha}_3+\frac{1}{3}\hat{\epsilon}_2^2\right]\delta\chi_a\right\}\\
& + v^5(1+3\log[v/v_{\rm LSO}])\left\{\left[-\frac{64160}{567}+\frac{93920}{567}\nu-\frac{1760}{189}\nu^2+\hat{\alpha}_2\left(\frac{160}{9}-\frac{1280}{81}\nu-\frac{160}{81}\nu^2\right)\right.\right.\\
& +\hat{\alpha}_3\left(-\frac{85600}{567}+\frac{12400}{81}\nu-\frac{22000}{567}\nu^2\right)+\hat{\alpha}_5\left(-\frac{1120}{9}+\frac{16940}{81}\nu-\frac{280}{81}\nu^2\right)\\
& +\left(\frac{13670}{1701}-\frac{58090}{1701}\nu+\frac{13640}{1701}\nu^2+\hat{\alpha}_3\left[\frac{68350}{1701}-\frac{34175}{189}\nu+\frac{136700}{1701}\nu^2\right]\right)\hat{\mu}_3^2+\left(\frac{6835}{6804}-\frac{13670}{1701}\nu+\frac{27340}{1701}\nu^2\right)\hat{\mu}_3^2\hat{\epsilon}_2^2\\
& +\left(-\frac{1465}{486}+\frac{23230}{1701}\nu-\frac{10880}{1701}\nu^2+\hat{\alpha}_2\left[\frac{5}{9}-\frac{175}{81}\nu-\frac{20}{81}\nu^2\right]+\hat{\alpha}_3\left[\frac{200}{243}-\frac{100}{27}\nu+\frac{400}{243}\nu^2\right]\right)\hat{\epsilon}_2^2\\
& +\left(\frac{5}{243}-\frac{40}{243}\nu+\frac{80}{243}\nu^2\right)\hat{\epsilon}_2^4+\left(\frac{1600}{567}\nu-\frac{1600}{189}\nu^2\right)\hat{\epsilon}_3^2\Big]\chi_s+\left[-\frac{64160}{567}+\frac{17440}{567}\nu+\hat{\alpha}_2\left(\frac{160}{9}+\frac{160}{81}\nu\right)\right.\\
& -\hat{\alpha}_3\left(\frac{85600}{567}-\frac{44000}{567}\nu\right)-\hat{\alpha}_5\left(\frac{1120}{9}-\frac{4340}{81}\nu\right)+\left(\frac{13670}{1701}-\frac{23930}{1701}\nu+\hat{\alpha}_3\left[\frac{68350}{1701}-\frac{273400}{1701}\nu\right]\right)\hat{\mu}_3^2\\
& +\left(\frac{6835}{6804}-\frac{6835}{1701}\nu\right)\hat{\mu}_3^2\hat{\epsilon}_2^2+\left(-\frac{1465}{486}+\frac{4520}{1701}\nu+\hat{\alpha}_2\left[\frac{5}{9}+\frac{5}{81}\nu\right]+\hat{\alpha}_3\left[\frac{200}{243}-\frac{800}{243}\nu\right]\right)\hat{\epsilon}_2^2+\left(\frac{5}{243}-\frac{20}{243}\nu\right)\hat{\epsilon}_2^4\Big]\delta\chi_a\Big\}\\
& +\pi v^6\left\{\left[\frac{640}{3}-\frac{640}{3}\nu+\hat{\alpha}_3\left(\frac{1600}{3}-\frac{800}{3}\nu\right)+(10-40\nu)\hat{\epsilon}_2^2\right]\chi_s+\left[\frac{640}{3}+10\hat{\epsilon}_2^2+\frac{1600}{3}\hat{\alpha}_3\right]\delta\chi_a\right\}\\
& +v^7\left\{\left[-\frac{175520}{63}+\frac{7871090}{1323}\nu-\frac{4100}{3}\nu^2-\frac{199520}{1323}\nu^3+\hat{\alpha}_2\left(\frac{16040}{21}-\frac{195280}{189}\nu-\frac{11600}{189}\nu^2+\frac{440}{63}\nu^3\right)\right.\right.\\
& +\hat{\alpha}_3\left(-\frac{11825200}{3969}+\frac{11267500}{3969}\nu-\frac{1322350}{1323}\nu^2+\frac{644800}{3969}\nu^3\right)+\hat{\alpha}_4\left(540-920\nu+\frac{1160}{3}\nu^2-\frac{20}{3}\nu^3\right)\\
& +\hat{\alpha}_5\left(-\frac{8560}{3}+\frac{169070}{27}\nu-\frac{68690}{27}\nu^2+\frac{1100}{27}\nu^3\right)+\hat{\alpha}_7\left(-2430+\frac{16785}{2}\nu-2580\nu^2-15\nu^3\right)\\
& +\hat{\mu}_3^2\left(\frac{58105}{189}-\frac{22900195}{15876}\nu+\frac{8056835}{10584}\nu^2+\frac{2844815}{7938}\nu^3\right)+\hat{\mu}_3^2\hat{\alpha}_2\left(-\frac{6835}{126}+\frac{127285}{567}\nu-\frac{32335}{1134}\nu^2-\frac{3410}{567}\nu^3\right)\\
& +\hat{\mu}_3^2\hat{\alpha}_3\left(\frac{524075}{1323}-\frac{5309275}{2646}\nu+\frac{2381500}{1323}\nu^2-\frac{592600}{1323}\nu^3\right)+\hat{\mu}_3^2\hat{\alpha}_5\left(\frac{6835}{9}-\frac{2795515}{648}\nu+\frac{20505}{4}\nu^2-\frac{6835}{81}\nu^3\right)\\
& +\hat{\mu}_3^2\hat{\epsilon}_2^2\left(\frac{3260435}{127008}-\frac{7054105}{31752}\nu+\frac{4326905}{7938}\nu^2-\frac{355490}{1323}\nu^3\right)+\hat{\mu}_3^2\hat{\epsilon}_2^2\hat{\alpha}_2\left(-\frac{6835}{1008}+\frac{485285}{9072}\nu-\frac{116195}{1134}\nu^2-\frac{6835}{567}\nu^3\right)\\
& +\hat{\mu}_3^2\hat{\epsilon}_2^2\hat{\alpha}_3\left(-\frac{34175}{3402}+\frac{580975}{6804}\nu-\frac{341750}{1701}\nu^2+\frac{136700}{1701}\nu^3\right)+\hat{\mu}_3^2\hat{\epsilon}_2^4\left(-\frac{6835}{18144}+\frac{6835}{1512}\nu-\frac{6835}{378}\nu^2+\frac{13670}{567}\nu^3\right)\\
& +\hat{\mu}_3^2\hat{\epsilon}_3^2\left(-\frac{136700}{3969}\nu+\frac{136700}{567}\nu^2-\frac{546800}{1323}\nu^3\right)+\hat{\mu}_3^4\left(-\frac{129865}{1764}\nu+\frac{259730}{441}\nu^2-\frac{519460}{441}\nu^3\right)\\
& +\hat{\mu}_3^4\hat{\epsilon}_2^2\left(-\frac{9343445}{1016064}+\frac{9343445}{84672}\nu-\frac{9343445}{21168}\nu^2+\frac{9343445}{15876}\nu^3\right)\\
& +\hat{\mu}_3^4\hat{\alpha}_3\left(-\frac{46717225}{190512}+\frac{794192825}{381024}\nu-\frac{233586125}{47628}\nu^2+\frac{46717225}{23814}\nu^3\right)\\
& +\hat{\mu}_4^2\left(\frac{289760}{11907}\nu-\frac{205600}{567}\nu^2+\frac{1149440}{1323}\nu^3\right)+\hat{\mu}_4^2\hat{\alpha}_3\left(\frac{3586000}{11907}-\frac{23309000}{11907}\nu+\frac{14344000}{3969}\nu^2-\frac{1793000}{1323}\nu^3\right)\\
& +\hat{\mu}_4^2\hat{\epsilon}_2^2\left(\frac{89650}{11907}-\frac{896500}{11907}\nu+\frac{986150}{3969}\nu^2-\frac{358600}{1323}\nu^3\right)+\hat{\epsilon}_2^2\left(-\frac{1193245}{15876}+\frac{938855}{2646}\nu-\frac{7469165}{31752}\nu^2+\frac{83995}{1134}\nu^3\right)
\end{aligned}
$$

$$
\begin{aligned}
&+\hat{\epsilon}_2^2\hat{\alpha}_2\left(\frac{1465}{72}-\frac{407885}{4536}\nu+\frac{5335}{162}\nu^2+\frac{2720}{567}\nu^3\right)+\hat{\epsilon}_2^2\hat{\alpha}_3\left(\frac{18850}{567}-\frac{92825}{567}\nu+\frac{73700}{567}\nu^2-\frac{16000}{567}\nu^3\right)\\
&+\hat{\epsilon}_2^2\hat{\alpha}_4\left(\frac{135}{8}-\frac{635}{8}\nu+\frac{1145}{24}\nu^2-\frac{5}{6}\nu^3\right)+\hat{\epsilon}_2^2\hat{\alpha}_5\left(\frac{140}{9}-\frac{14315}{162}\nu+105\nu^2-\frac{140}{81}\nu^3\right)\\
&+\hat{\epsilon}_2^2\hat{\epsilon}_3^2\left(\frac{50}{189}-\frac{1900}{567}\nu+\frac{7750}{567}\nu^2-\frac{3400}{189}\nu^3\right)+\hat{\epsilon}_2^4\left(\frac{1745}{1512}-\frac{1585}{162}\nu+\frac{12970}{567}\nu^2-\frac{5000}{567}\nu^3\right)\\
&+\hat{\epsilon}_2^4\hat{\alpha}_2\left(-\frac{5}{36}+\frac{355}{324}\nu-\frac{170}{81}\nu^2-\frac{20}{81}\nu^3\right)+\hat{\epsilon}_2^4\hat{\alpha}_3\left(-\frac{25}{243}+\frac{425}{486}\nu-\frac{500}{243}\nu^2+\frac{200}{243}\nu^3\right)\\
&+\hat{\epsilon}_2^6\left(-\frac{5}{1296}+\frac{5}{108}\nu-\frac{5}{27}\nu^2+\frac{20}{81}\nu^3\right)+\hat{\epsilon}_3^2\left(\frac{258520}{3969}\nu-\frac{966200}{3969}\nu^2+\frac{612800}{3969}\nu^3\right)\\
&+\hat{\epsilon}_3^2\hat{\alpha}_2\left(-\frac{400}{21}\nu+\frac{10400}{189}\nu^2+\frac{400}{63}\nu^3\right)+\hat{\epsilon}_3^2\hat{\alpha}_3\left(\frac{2000}{189}-\frac{13000}{189}\nu+\frac{8000}{63}\nu^2-\frac{1000}{21}\nu^3\right)\\
&+\hat{\epsilon}_4^2\left(\frac{28705}{1764}\nu-\frac{28705}{294}\nu^2+\frac{57410}{441}\nu^3\right)\Bigg]\chi_s\\
&+\Bigg[-\frac{175520}{63}+\frac{3039410}{1323}\nu+\frac{29300}{1323}\nu^2+\hat{\alpha}_2\left(\frac{16040}{21}-\frac{23200}{189}\nu-\frac{4360}{189}\nu^2\right)+\hat{\alpha}_3\left(-\frac{11825200}{3969}+\frac{5354900}{3969}\nu-\frac{1289600}{3969}\nu^2\right)\\
&+\hat{\alpha}_4\left(540-380\nu+\frac{20}{3}\nu^2\right)+\hat{\alpha}_5\left(-\frac{8560}{3}+\frac{72770}{27}\nu-\frac{17050}{27}\nu^2\right)+\hat{\alpha}_7\left(-2430+\frac{9495}{2}\nu-105\nu^2\right)\\
&+\hat{\mu}_3^2\left(\frac{58105}{189}-\frac{15599425}{15876}\nu-\frac{5525}{24}\nu^2\right)+\hat{\mu}_3^2\hat{\alpha}_2\left(-\frac{6835}{126}+\frac{50425}{567}\nu+\frac{11965}{1134}\nu^2\right)\\
&+\hat{\mu}_3^2\hat{\alpha}_3\left(\frac{524075}{1323}-\frac{341800}{189}\nu+\frac{1185200}{1323}\nu^2\right)+\hat{\mu}_3^2\hat{\alpha}_5\left(\frac{6835}{9}-\frac{2180365}{648}\nu+\frac{211885}{162}\nu^2\right)\\
&+\hat{\mu}_3^2\hat{\epsilon}_2^2\left(\frac{3260435}{127008}-\frac{2245385}{15876}\nu+\frac{1230335}{7938}\nu^2\right)+\hat{\mu}_3^2\hat{\epsilon}_2^2\hat{\alpha}_2\left(-\frac{6835}{1008}+\frac{34175}{1296}\nu+\frac{6835}{2268}\nu^2\right)\\
&+\hat{\mu}_3^2\hat{\epsilon}_2^2\hat{\alpha}_3\left(-\frac{34175}{3402}+\frac{136700}{1701}\nu-\frac{273400}{1701}\nu^2\right)+\hat{\mu}_3^2\hat{\epsilon}_2^4\left(-\frac{6835}{18144}+\frac{6835}{2268}\nu-\frac{6835}{1134}\nu^2\right)\\
&+\hat{\mu}_3^4\left(-\frac{7005875}{31752}\nu+\frac{7005875}{7938}\nu^2\right)+\hat{\mu}_3^4\hat{\alpha}_3\left(-\frac{46717225}{190512}+\frac{46717225}{23814}\nu-\frac{46717225}{11907}\nu^2\right)\\
&+\hat{\mu}_3^4\hat{\epsilon}_2^2\left(-\frac{9343445}{1016064}+\frac{9343445}{127008}\nu-\frac{9343445}{63504}\nu^2\right)+\hat{\mu}_4^2\left(\frac{31840}{147}\nu-\frac{31840}{49}\nu^2\right)+\hat{\mu}_4^2\hat{\alpha}_3\left(\frac{3586000}{11907}-\frac{7172000}{3969}\nu+\frac{3586000}{1323}\nu^2\right)\\
&+\hat{\mu}_4^2\hat{\epsilon}_2^2\left(\frac{89650}{11907}-\frac{179300}{3969}\nu+\frac{89650}{1323}\nu^2\right)+\hat{\epsilon}_2^2\left(-\frac{1193245}{15876}+\frac{65255}{882}\nu-\frac{1742365}{31752}\nu^2\right)\\
&+\hat{\epsilon}_2^2\hat{\alpha}_2\left(\frac{1465}{72}-\frac{71105}{4536}\nu-\frac{1130}{567}\nu^2\right)+\hat{\epsilon}_2^2\hat{\alpha}_3\left(\frac{18850}{567}-\frac{27800}{189}\nu+\frac{32000}{567}\nu^2\right)+\hat{\epsilon}_2^2\hat{\alpha}_4\left(\frac{135}{8}-\frac{95}{8}\nu+\frac{5}{24}\nu^2\right)\\
&+\hat{\epsilon}_2^2\hat{\alpha}_5\left(\frac{140}{9}-\frac{11165}{162}\nu+\frac{2170}{81}\nu^2\right)+\hat{\epsilon}_2^2\hat{\epsilon}_3^2\left(\frac{50}{189}-\frac{100}{63}\nu+\frac{50}{21}\nu^2\right)+\hat{\epsilon}_2^4\left(\frac{1745}{1512}-\frac{50}{9}\nu+\frac{710}{189}\nu^2\right)\\
&+\hat{\epsilon}_2^4\hat{\alpha}_2\left(-\frac{5}{36}+\frac{175}{324}\nu+\frac{5}{81}\nu^2\right)+\hat{\epsilon}_2^4\hat{\alpha}_3\left(-\frac{25}{243}+\frac{200}{243}\nu-\frac{400}{243}\nu^2\right)-\hat{\epsilon}_2^6\left(\frac{5}{1296}-\frac{5}{162}\nu+\frac{5}{81}\nu^2\right)+\hat{\epsilon}_3^2\left(\frac{3800}{189}\nu-\frac{3800}{63}\nu^2\right)\\
&+\hat{\epsilon}_3^2\hat{\alpha}_3\left(\frac{2000}{189}-\frac{4000}{63}\nu+\frac{2000}{21}\nu^2\right)-\hat{\epsilon}_4^2\left(\frac{28705}{1764}\nu-\frac{28705}{882}\nu^2\right)\Bigg]\delta\chi_a\Bigg\} \qquad (3.9)
\end{aligned}
$$

$$
\begin{aligned}
\psi_{\rm SS}(f) = v^4 \Bigg\{ & \left[-10\kappa_+ - \frac{5}{8}\hat{\epsilon}_2^2 - 15\kappa_+\hat{\alpha}_4 - \delta\kappa_-(10+15\hat{\alpha}_4) + \left(-40+20\kappa_+ + \frac{5}{2}\hat{\epsilon}_2^2 - \hat{\alpha}_4[60-30\kappa_+]\right)\nu \right]\chi_s^2 \\
& + \left[-20\kappa_- - 30\kappa_-\hat{\alpha}_4 - \delta\left(20\kappa_+ + 30\kappa_+\hat{\alpha}_4 + \frac{5}{4}\hat{\epsilon}_2^2\right) + \nu\kappa_-(40+60\hat{\alpha}_4)\right]\chi_s\chi_a \\
& + \left[-10\kappa_+ - \frac{5}{8}\hat{\epsilon}_2^2 - 15\kappa_+\hat{\alpha}_4 - \delta\kappa_-(10+15\hat{\alpha}_4) + (40+20\kappa_+ + \hat{\alpha}_4[60+30\kappa_+])\nu \right]\chi_a^2 \Bigg\} \\
& + v^6 \Bigg\{ \left[-\frac{1120}{9} + \frac{1150}{7}\kappa_+ + \kappa_-\delta\left(\frac{1150}{7} - \frac{690}{7}\nu\right) + \left(\frac{38600}{63} - \frac{2990}{7}\kappa_+\right)\nu \right. \\
& - \left(\frac{3880}{21} - \frac{1940}{21}\kappa_+\right)\nu^2 + \frac{1600}{63}\nu^2\hat{\epsilon}_3^2 + \hat{\alpha}_2\left(-30\kappa_+ - \left[30+\frac{10}{3}\nu\right]\delta\kappa_- + \left[-120+\frac{170}{3}\kappa_+\right]\nu + \left[-\frac{40}{3}+\frac{20}{3}\kappa_+\right]\nu^2\right) \\
& - \hat{\alpha}_3\left(\frac{3200}{9} - \frac{1600}{3}\nu + \frac{1600}{9}\nu^2\right) + \hat{\alpha}_4\left(\frac{1070}{7}\kappa_+ + \left[\frac{1070}{7} - \frac{550}{7}\nu\right]\delta\kappa_- + \left[\frac{4280}{7} - \frac{2690}{7}\kappa_+\right]\nu - \left[\frac{2200}{7} - \frac{1100}{7}\kappa_+\right]\nu^2\right) \\
& + \hat{\alpha}_6\left(-\frac{1600}{9} + \frac{700}{3}\kappa_+ + \left[\frac{700}{3} - \frac{500}{3}\nu\right]\delta\kappa_- + \left[\frac{1600}{9} - \frac{1900}{3}\kappa_+\right]\nu + \left[\frac{2000}{9} + \frac{200}{3}\kappa_+\right]\nu^2\right) \\
& + \hat{\mu}_3^2\left(-\frac{95}{7}\kappa_+ + \left[-\frac{95}{7} + \frac{13675}{252}\nu\right]\delta\kappa_- + \left[-\frac{6835}{126} + \frac{20515}{252}\kappa_+\right]\nu + \left[\frac{13670}{63} - \frac{6835}{63}\kappa_+\right]\nu^2\right) \\
& + \hat{\mu}_3^2\hat{\alpha}_4\left(-\frac{6835}{168}\kappa_+ - \left[\frac{6835}{168} - \frac{6835}{42}\nu\right]\delta\kappa_- - \left[\frac{6835}{42} - \frac{6835}{28}\kappa_+\right]\nu + \left[\frac{13670}{21} - \frac{6835}{21}\kappa_+\right]\nu^2\right) \\
& - \hat{\mu}_3^2\hat{\epsilon}_2^2\left(\frac{6835}{2016} - \frac{6835}{252}\nu + \frac{6835}{126}\nu^2\right) + \hat{\epsilon}_2^2\left(\frac{470}{63} - \frac{5}{6}\kappa_+ - \left[\frac{5}{6} - \frac{20}{9}\nu\right]\delta\kappa_- - \left[\frac{730}{21} - \frac{35}{9}\kappa_+\right]\nu + \left[\frac{1240}{63} - \frac{20}{9}\kappa_+\right]\nu^2\right) \\
& - \hat{\epsilon}_2^2\hat{\alpha}_2\left(\frac{15}{8} - \frac{175}{24}\nu - \frac{5}{6}\nu^2\right) - \hat{\epsilon}_2^2\hat{\alpha}_3\left(\frac{100}{9} - 50\nu + \frac{200}{9}\nu^2\right) + \hat{\epsilon}_2^2\hat{\alpha}_4\left(-\frac{5}{6}\kappa_+ - \left[\frac{5}{6} - \frac{10}{3}\nu\right]\delta\kappa_- - \left[\frac{10}{3} - 5\kappa_+\right]\nu \right. \\
& \left. + \left[\frac{40}{3} - \frac{20}{3}\kappa_+\right]\nu^2\right) - \hat{\epsilon}_2^4\left(\frac{5}{24} - \frac{5}{3}\nu + \frac{10}{3}\nu^2\right)\Bigg]\chi_s^2 + \left[\left(\frac{2300}{7} - \frac{5980}{7}\nu + \frac{3880}{21}\nu^2\right)\kappa_- \right. \\
& + \left(-\frac{2240}{9} + \frac{2300}{7}\kappa_+ + \left(\frac{560}{9} - \frac{1380}{7}\kappa_+\right)\nu\right)\delta + \hat{\alpha}_2\left(\left[-60 + \frac{340}{3}\nu + \frac{40}{3}\nu^2\right]\kappa_- - \left(60 + \frac{20}{3}\nu\right)\delta\kappa_+\right) \\
& - \hat{\alpha}_3\delta\left(\frac{6400}{9} - \frac{1600}{3}\nu\right) + \hat{\alpha}_4\left(\left[\frac{2140}{7} - \frac{5380}{7}\nu + \frac{2200}{7}\nu^2\right]\kappa_- + \left[\frac{2140}{7} - \frac{1100}{7}\nu\right]\kappa_+\delta\right) + \hat{\alpha}_6\left(\left[\frac{1400}{3} - \frac{3800}{3}\nu + \frac{400}{3}\nu^2\right]\kappa_- \right. \\
& \left. + \left[-\frac{3200}{9} + \frac{1400}{3}\kappa_+ - \left(\frac{5600}{9} + \frac{1000}{3}\kappa_+\right)\nu\right]\delta\right) + \hat{\mu}_3^2\left(\left[-\frac{190}{7} + \frac{20515}{126}\nu - \frac{13670}{63}\nu^2\right]\kappa_- + \left[-\frac{190}{7} + \frac{13675}{126}\nu\right]\delta\kappa_+\right) \\
& + \hat{\mu}_3^2\hat{\alpha}_4\left(\left[-\frac{6835}{84} + \frac{6835}{14}\nu - \frac{13670}{21}\nu^2\right]\kappa_- - \left[\frac{6835}{84} - \frac{6835}{21}\nu\right]\delta\kappa_+\right) - \hat{\mu}_3^2\hat{\epsilon}_2^2\delta\left(\frac{6835}{1008} - \frac{6835}{252}\nu\right) \\
& + \hat{\epsilon}_2^2\left(\left[-\frac{5}{3} + \frac{70}{9}\nu - \frac{40}{9}\nu^2\right]\kappa_- + \left[\frac{940}{63} - \frac{5}{3}\kappa_+ - \left(\frac{650}{63} - \frac{40}{9}\kappa_+\right)\nu\right]\delta\right) - \hat{\epsilon}_2^2\hat{\alpha}_2\delta\left(\frac{15}{4} + \frac{5}{12}\nu\right) - \hat{\epsilon}_2^2\hat{\alpha}_3\delta\left(\frac{200}{9} - 50\nu\right) \\
& + \hat{\epsilon}_2^2\hat{\alpha}_4\left(\left[-\frac{5}{3} + 10\nu - \frac{40}{3}\nu^2\right]\kappa_- + \left[-\frac{5}{3} + \frac{20}{3}\nu\right]\delta\kappa_+\right) - \hat{\epsilon}_2^4\delta\left(\frac{5}{12} - \frac{5}{3}\nu\right)\Bigg]\chi_s\chi_a \\
& + \left[-\frac{1120}{9} + \frac{1150}{7}\kappa_+ - \left(\frac{3320}{63} + \frac{2990}{7}\kappa_+\right)\nu + \left(\frac{3880}{21} + \frac{1940}{21}\kappa_+\right)\nu^2 + \left(\frac{1150}{7} - \frac{690}{7}\nu\right)\delta\kappa_- \right. \\
& + \hat{\alpha}_2\left(-30\kappa_+ + \left[120 + \frac{170}{3}\kappa_+\right]\nu + \left[\frac{40}{3} + \frac{20}{3}\kappa_+\right]\nu^2 - \left[30 + \frac{10}{3}\nu\right]\delta\kappa_-\right) - \hat{\alpha}_3\left(\frac{3200}{9} - \frac{12800}{9}\nu\right) \\
& \left. + \hat{\alpha}_4\left(\frac{1070}{7}\kappa_+ - \left[\frac{4280}{7} + \frac{2690}{7}\kappa_+\right]\nu + \left[\frac{2200}{7} + \frac{1100}{7}\kappa_+\right]\nu^2 + \left[\frac{1070}{7} - \frac{550}{7}\nu\right]\delta\kappa_-\right)
\end{aligned}
$$

$$+\hat{\alpha}_6\left(-\frac{1600}{9}+\frac{700}{3}\kappa_+-\left[\frac{800}{9}+\frac{1900}{3}\kappa_+\right]\nu+\left[\frac{400}{3}+\frac{200}{3}\kappa_+\right]\nu^2+\left[\frac{700}{3}-\frac{500}{3}\nu\right]\delta\kappa_-\right)$$
$$+\hat{\mu}_3^2\left(-\frac{95}{7}\kappa_++\left[\frac{6835}{126}+\frac{20515}{252}\kappa_+\right]\nu-\left[\frac{13670}{63}+\frac{6835}{63}\kappa_+\right]\nu^2-\left[\frac{95}{7}-\frac{13675}{252}\nu\right]\delta\kappa_-\right)$$
$$+\hat{\mu}_3^2\hat{\alpha}_4\left(-\frac{6835}{168}\kappa_++\left[\frac{6835}{42}+\frac{6835}{28}\kappa_+\right]\nu-\left[\frac{13670}{21}+\frac{6835}{21}\kappa_+\right]\nu^2-\left[\frac{6835}{168}-\frac{6835}{42}\nu\right]\delta\kappa_-\right)$$
$$+\hat{\mu}_3^2\hat{\epsilon}_2^2\left(-\frac{6835}{2016}+\frac{6835}{504}\nu\right)+\hat{\epsilon}_2^2\left(\frac{470}{63}-\frac{5}{6}\kappa_+-\left[\frac{340}{63}-\frac{35}{9}\kappa_+\right]\nu-\left[\frac{40}{9}+\frac{20}{9}\kappa_+\right]\nu^2-\left[\frac{5}{6}-\frac{20}{9}\nu\right]\delta\kappa_-\right)$$
$$-\hat{\epsilon}_2^2\hat{\alpha}_2\left(\frac{15}{8}+\frac{5}{24}\nu\right)-\hat{\epsilon}_2^2\hat{\alpha}_3\left(\frac{100}{9}-\frac{400}{9}\nu\right)+\hat{\epsilon}_2^2\hat{\alpha}_4\left(-\frac{5}{6}\kappa_++\left[\frac{10}{3}+5\kappa_+\right]\nu-\left[\frac{40}{3}+\frac{20}{3}\kappa_+\right]\nu^2-\left[\frac{5}{6}-\frac{10}{3}\nu\right]\delta\kappa_-\right)$$
$$-\hat{\epsilon}_2^4\left(\frac{5}{24}-\frac{5}{6}\nu\right)\Bigg]\chi_a^2\Bigg\} \tag{3.10}$$

As a consistency check, we confirm the recovery of the corresponding GR expression for the TaylorF2 phasing for aligned spin binaries (see Refs. [53,91,92]) in the limit, $\mu_2=\mu_3=\mu_4=\mu_5=\epsilon_2=\epsilon_3=\epsilon_4=\alpha_0=\alpha_2=\alpha_3=\alpha_4=\alpha_5=\alpha_6=\alpha_7=1$. We also update Table I of Ref. [37] to explicitly show the appearances of the parameters μ_l and ϵ_l at various PN order of the phasing formula (see Table I).

One of the salient features of the parametrized multipolar spinning phasing derived here is the presence of ϵ_2 at 1.5PN order and ϵ_3 at 2.5PN order (logarithmic) due to the spin-orbit interactions and hence not present in the nonspinning phasing. Though at 2PN and 3PN order, due to the spin-spin interactions, there are no additional multipole moments compared to the nonspinning systems, these are the orders at which $\kappa_{+,-}$ appear. This has an interesting interpretation as $\kappa_{+,-}$ can be thought of as parametrizing potential deviations from BH nature [93,94] as binaries comprising of non-BHs will have $\kappa_{+,-}$ to be different from 2 and 0, respectively, which are the unique values corresponding to binary black holes. The cross-terms of the multipole coefficients with $\kappa_{+,-}$ showcase the degeneracy between binary black holes in alternative theories and non-BHs in GR. As one can see from Eq. (3.10), μ_2, μ_3, and ϵ_2 are the multipole coefficients which are sensitive to the non-BH nature (vis-a-vis the above mentioned parametrization). As can be seen from the phasing formula, these imprints will be higher order corrections to the multipole coefficients and may not influence their estimates unless the values of $\kappa_{+,-}$ are sufficiently high.

TABLE I. Update of the summary given in Table I of Ref. [37] for the multipolar structure of the PN phasing formula. Contribution of various multipoles to different phasing coefficients and their frequency dependences are tabulated. The additional multipole coefficients appearing due to spin are underlined. Following the definitions introduced in Ref. [37], μ_l refer to mass-type multipole moments and ϵ_l refer to current-type multipole moments.

PN order	Frequency dependences	Multipole coefficients
0 PN	$f^{-5/3}$	μ_2
1 PN	f^{-1}	μ_2, μ_3, ϵ_2
1.5 PN	$f^{-2/3}$	μ_2, $\underline{\epsilon_2}$
2 PN	$f^{-1/3}$	μ_2, μ_3, μ_4, ϵ_2, ϵ_3
2.5 PN log	$\log f$	μ_2, μ_3, ϵ_2, $\underline{\epsilon_3}$
3 PN	$f^{1/3}$	μ_2, μ_3, μ_4, μ_5, ϵ_2, ϵ_3, ϵ_4
3 PN log	$f^{1/3}\log f$	μ_2
3.5 PN	$f^{2/3}$	μ_2, μ_3, μ_4, ϵ_2, ϵ_3, $\underline{\epsilon_4}$

IV. PARAMETER ESTIMATION SCHEME

In this section, we briefly describe the semianalytical Fisher information matrix based parameter estimation scheme [95–98] used in our analysis. We also discuss the leading order bounds on the systematics of the estimated parameters due to the difference between the spinning and nonspinning waveforms in the Appendix for LISA.

For $\vec{\theta}$ being the set of parameters defining the GW signal $\tilde{h}(f;\vec{\theta})$, the Fisher information matrix is defined as

$$\Gamma_{mn}=\left\langle\frac{\partial\tilde{h}(f;\vec{\theta})}{\partial\theta_m},\frac{\partial\tilde{h}(f;\vec{\theta})}{\partial\theta_n}\right\rangle, \tag{4.1}$$

where $\langle\ldots,\ldots\rangle$ is the inner product weighted by the detector noise. To be precise,

$$\langle a,b\rangle=2\int_{f_{\rm low}}^{f_{\rm high}}\frac{a(f)b^*(f)+a^*(f)b(f)}{S_h(f)}df. \tag{4.2}$$

Here "$*$" denotes the complex conjugation and $S_h(f)$ is the one-sided noise power spectral density (PSD) of the detector while $f_{\rm low}$ and $f_{\rm high}$ denote the lower and upper limits of the integration. Though $f_{\rm low}$ arises from the detector sensitivity, $f_{\rm high}$ is defined by the frequency at the last stable orbit of the binary beyond which the PN approximation would break down. In the large signal-to-noise ratio (SNR) limit, the distribution of the inferred parameters follow a Gaussian distribution around their respective true values for which the variance-covariance matrix of the errors on the parameters is simply the inverse of the Fisher matrix,

$$C^{mn} = (\Gamma^{-1})^{mn},$$

and the 1σ statistical error is, $\Delta_{\rm stat}\theta_m = \sqrt{C^{mm}}$.

Fisher information matrix method, by default, assumes a flat prior distribution in the range $[-\infty, \infty]$ on all the parameters to be estimated [97,99]. In contrast, in the large SNR limit, a Gaussian prior can also be implemented on the desired parameter as described in Ref. [97]. For our purpose, we employ a Gaussian prior on ϕ_c centered around $\phi_c = 0$ with a variance of about π^2. This choice is somewhat adhoc but ensures that the width of the Gaussian is not too small to significantly influence the result but helps us deal with the ill-conditionedness of the Fisher matrix. This also restricts the prior range to exceed to the unphysical domain beyond $\pm\pi$. Hence our modified Fisher matrix has the following form,

$$\Gamma' = \Gamma + \Gamma^{(0)}, \tag{4.3}$$

where $\Gamma^{(0)}$ is a diagonal matrix with only one nonzero element corresponding to $\Gamma^{(0)}_{\phi_c\phi_c}$ component. We use this modified Fisher matrix (Γ') for the estimation of 1σ statistical errors which also can be interpreted as the 1σ upper bounds on any deviation of these coefficients from GR value.

We estimate the statistical errors on various multipole coefficients while considering an eight dimensional parameter space, $\{t_c, \phi_c, \log\mathcal{A}, \log\mathcal{M}_c, \log\nu, \chi_s, \chi_a, \mu_\ell \text{ or } \epsilon_\ell \text{ or } \alpha_m\}$ to specify the true GW signal.

V. DETECTOR CONFIGURATIONS

We describe here the various detector configurations we considered in the present study.

A. Ground-based second generation detector network

As a representative case, we consider a worldwide network of five second-generation ground based detectors: LIGO-Hanford, LIGO-Livingston, Virgo, KAGRA [100], and LIGO-India [101]. We assume the noise PSD for LIGO-Hanford, LIGO-Livingstone and LIGO-India to be the analytical fit given in Ref. [102] whereas the following fit is used for Virgo PSD,

$$\begin{aligned} S_h^{\rm virgo}(f) = 1.5344\times10^{-47}\Bigg[&1 + 1871\times\left(\frac{16}{f}\right)^{10} \\ &+ 11.72\times\left(\frac{30}{f}\right)^{6} + 0.7431\times\left(\frac{50}{f}\right)^{2} \\ &+ 0.9404\times\left(\frac{70}{f}\right) + 0.2107\times\left(\frac{100}{f}\right)^{0.5} \\ &+ 26.02\left(\frac{f}{500}\right)^{2}\Bigg]\ {\rm Hz}^{-1}, \end{aligned} \tag{5.1}$$

where f is in units of Hz. We consider the lower cut off frequency $\rm f_{low} = 10$ Hz for these detectors. For the Japanese detector KAGRA we use the noise PSD given in Ref. [103] with $\rm f_{low} = 1$ Hz. For all the detectors, $f_{\rm high}$ is taken to be the frequency at the last stable orbit, $f_{\rm LSO} = 1/(\pi m 6^{3/2})$. As opposed to the single detector Fisher matrix analysis, for a network of detectors, the Fisher matrix is evaluated for each detector and then added to obtain the network-Fisher-matrix. To estimate the individual Fisher matrices we use a waveform that is weighted with the correct antenna pattern functions $F_{+/\times}(\theta,\phi,\psi)$ of the detectors, where θ, ϕ, and ψ are the declination, the right ascension and the polarization angle of the source in the sky. More precisely we use the following waveform

$$\begin{aligned} \tilde{h}(f) = &\frac{1+\cos^2\iota}{2}F_+(\theta,\phi,\psi)\tilde{h}_+(f) \\ &+ \cos\iota F_\times(\theta,\phi,\psi)\tilde{h}_\times(f) \end{aligned} \tag{5.2}$$

with

$$\tilde{h}_+(f) = \mathcal{A}\mu_2 f^{-7/6}e^{-i\Psi_s}, \tag{5.3}$$

$$\tilde{h}_\times(f) = -i\tilde{h}_+(f). \tag{5.4}$$

The individual $F_{+/\times}(\theta,\phi,\psi)$ for each detector are estimated incorporating their location on Earth and Earth's rotation as given in Ref. [104]. We calculate the Fisher matrix for each detector considering an eight dimensional parameter space, $\{t_c, \phi_c, \log\mathcal{A}, \log\mathcal{M}_c, \log\nu, \chi_s, \chi_a, \mu_\ell \text{ or } \epsilon_\ell \text{ or } \alpha_m\}$ specifying the GW signal. Here we fix the four angles, $\theta, \phi, \psi, \iota$ to be $\pi/6, \pi/3, \pi/6, \pi/5$ respectively and do not treat them as parameters in the Fisher matrix estimation. These four angles, being the extrinsic parameters, have small correlation with the intrinsic ones especially with the multipole or the energy coefficients, and hence have negligible effect on their measurement.

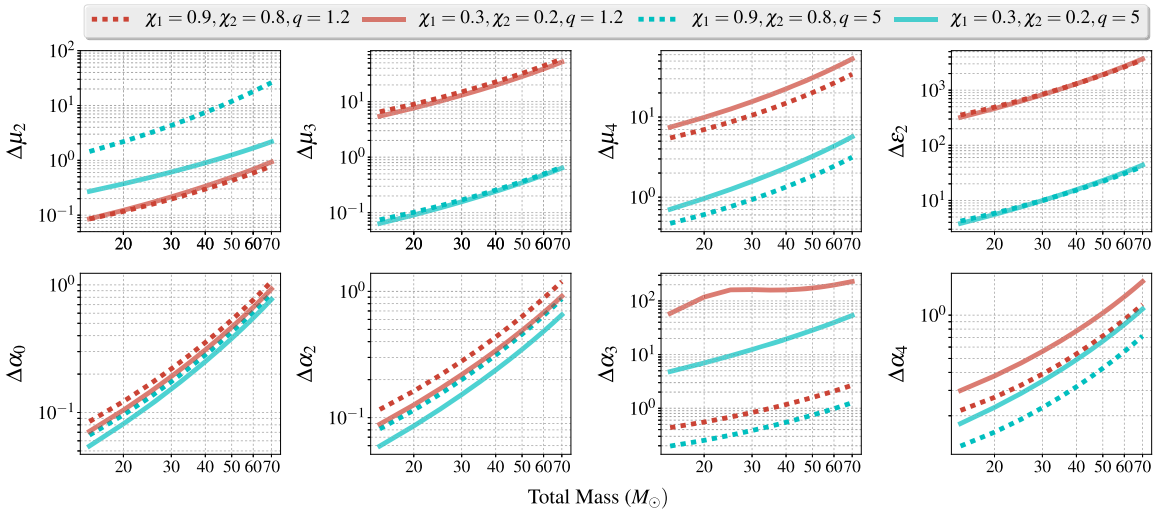

FIG. 1. Projected 1σ errors on the multipole and the energy coefficients as a function of total mass for two different mass ratios $q = m_1/m_2 = 1.2$, 5 and two spin configurations, $\chi_1 = 0.9$, $\chi_2 = 0.8$ and $\chi_1 = 0.3$, $\chi_2 = 0.2$ for the second generation detector network. All the sources are at a fixed luminosity distance of 100 Mpc with the angular position and orientations to be $\theta = \pi/6, \phi = \pi/3, \psi = \pi/6, \iota = \pi/5$. To obtain the numerical estimates showed in this plot, we also consider a prior distribution on ϕ_c. To be precise, we assume the prior on ϕ_c for each detector in the network to follow a Gaussian distribution with a zero mean and a variance of $1/\pi^2$.

B. Ground-based third generation detector network

As a representative case for the third generation ground-based detector network, we consider three detectors: one Cosmic Explorer-wide band (CE-wb) [105] in Australia, one CE-wb in Utah-USA, and one Einstein Telescope-D (ET-D) [106] in Europe. We use the noise PSD given in Ref. [106] for ET-D and the analytical fit given in Ref. [37] for the CE-wb. We assume $f_{\rm low}$ to be 1 and 5 Hz for the ET-D and CE-wb, respectively. To evaluate the Fisher matrix for this network configuration we use the same waveform as given in Eq. (5.2) except for the estimation of Fisher matrix in case of ET-D, we multiply the waveform by $\sin(\pi/3)$ because of its triangular shape. We follow the same scheme as described in Sec. V A to estimate the 1σ bounds on μ_2, μ_3, μ_4, ϵ_2 and α_0, α_2, α_3, α_4.

C. Space-based LISA detector

For the space-based detector, LISA, we use analytical fit given in [107] and choose $f_{\rm low}$ in such a way that the signal stays in the detector band for one year or less depending on the frequency at the last stable orbit. More specifically, we assume $f_{\rm low}$ to be [90,108]

$$f_{\rm low} = \max\left[10^{-5}, 4.149\times10^{-5}\left(\frac{\mathcal{M}_c}{10^6\ M_\odot}\right)^{-5/8} \times\left(\frac{T_{\rm obs}}{1\ \rm yr}\right)^{-3/8}\right], \tag{5.5}$$

where $T_{\rm obs}$ is the observation time which we consider to be one year. We assume the upper cutoff frequency, $f_{\rm high}$, to be the minimum of $[0.1, f_{\rm LSO}]$. The waveform we employ for LISA is given in Eq. (3.3) except we multiply it by an additional factor of $\sqrt{3}/2$ in order to account for the triangular shape of the detector. We do not account for the orbital motion of LISA in our calculations and consider LISA to be a single detector.

We next discuss the Fisher matrix projections for the various deformation coefficients parametrizing the conservative and dissipative sectors in the context of advanced ground-based and space-based gravitational wave detectors.

VI. RESULTS

Our results for the ground-based detectors are depicted in Figs. 1 (second generation) and 2 (third generation) and those for the space-based LISA detector are presented in Figs. 3–7. For the second and third generation ground-based detectors configurations, we choose the binary systems with two different mass ratios $q = 1.2$, 5 for two sets of spin configurations: high spin case ($\chi_1 = 0.9$, $\chi_2 = 0.8$) and low spin case ($\chi_1 = 0.3$, $\chi_2 = 0.2$). We also assume the luminosity distance to all these prototypical sources to be 100 Mpc. We consider these sources are detected with a network of second or third generation detectors as detailed in the last section. For LISA, we consider our prototypical supermassive BHs to be at the luminosity distance of 3 Gpc with three different mass ratios of $q = 1.2$, 5, 10. For these mass ratios, we

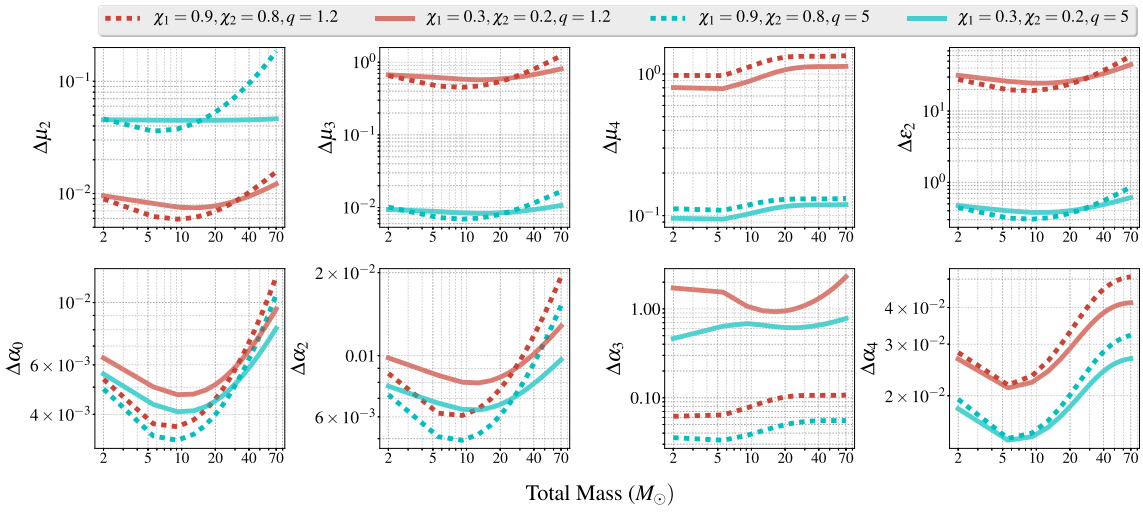

FIG. 2. Projected 1σ errors on the multipole and the energy coefficients as a function of total mass for two different mass ratios $q = m_1/m_2 = 1.2, 5$ and two spin configurations, $\chi_1 = 0.9, \chi_2 = 0.8$ and $\chi_1 = 0.3, \chi_2 = 0.2$ for the third generation detector network. All the sources are at a fixed luminosity distance of 100 Mpc with the angular position and orientations to be $\theta = \pi/5, \phi = \pi/6, \psi = \pi/4, \iota = \pi/4$. To obtain the numerical estimates showed in this plot, we also consider a prior distribution on ϕ_c. To be precise, we assume the prior on ϕ_c for each detector in the network to follow a Gaussian distribution with a zero mean and a variance of $1/\pi^2$.

investigate both high spin ($\chi_1 = 0.9$, $\chi_2 = 0.8$) and low spin ($\chi_1 = 0.3$, $\chi_2 = 0.2$) scenarios.

First we discuss the qualitative features in the plots. As expected, the third generation detector network which has better band width and sensitivity does better than the second generation detectors whereas LISA and third generation detectors perform comparably, though for totally different source configurations. The bounds on the multipole coefficients describing the dissipative dynamics broadly follows the trends seen in the nonspinning study carried out in Ref. [37]. The mass-type multipole moments are measured better than the current-type ones appearing at

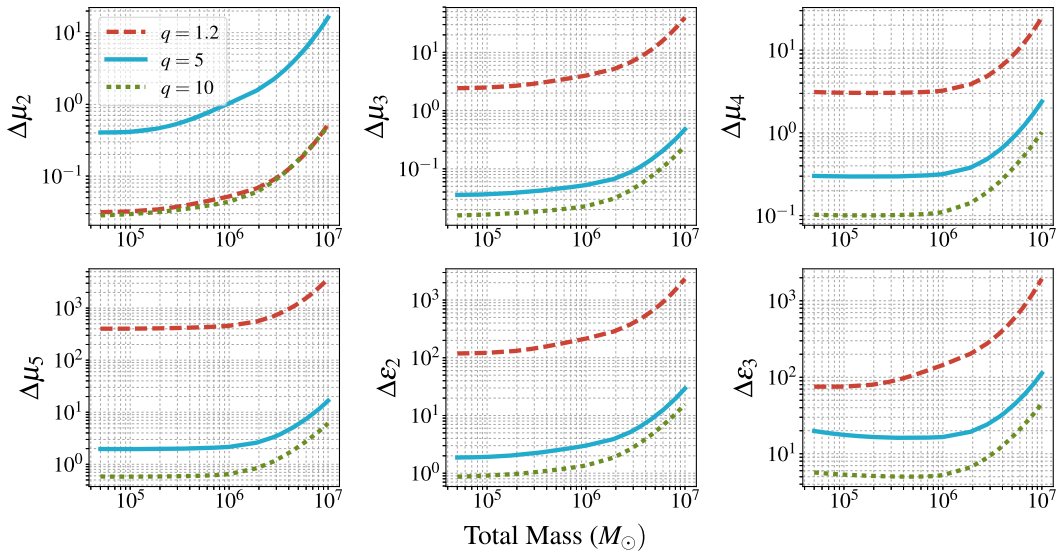

FIG. 3. Projected 1σ errors on the multipole coefficients as a function of total mass for three different mass ratios $q = m_1/m_2 = 1.2, 5$, and 10 in case of LISA noise PSD. We assume $\chi_1 = 0.9, \chi_2 = 0.8$. All the sources are considered to be at a fixed luminosity distance of 3 Gpc. To obtain the numerical estimates showed in this plot, we also consider a prior distribution on ϕ_c. To be precise, we assume ϕ_c to follow a Gaussian distribution with a zero mean and a variance of $1/\pi^2$.

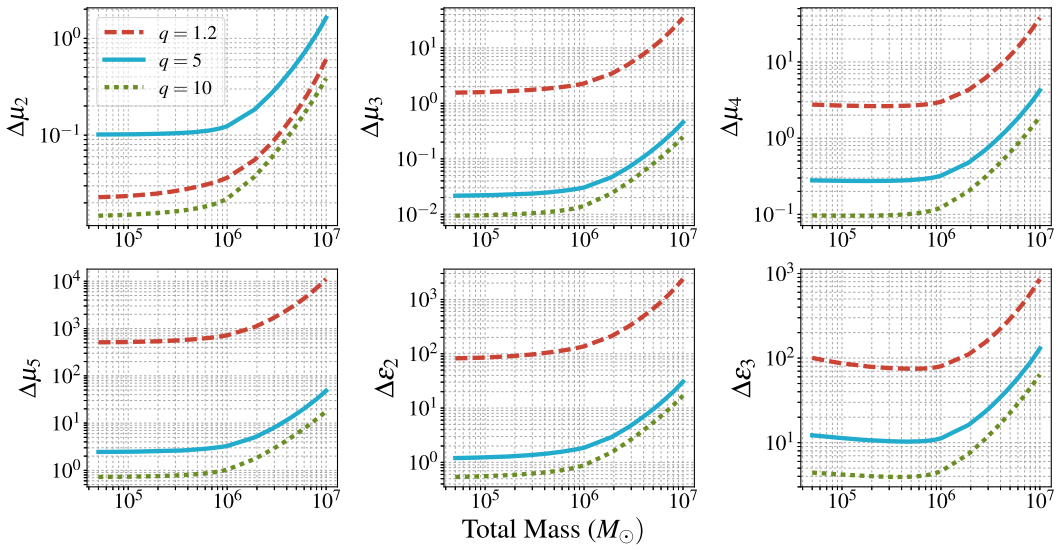

FIG. 4. Projected 1σ errors on the multipole coefficients as a function of total mass for three different mass ratios $q = m_1/m_2 = 1.2, 5,$ and 10 in case of LISA noise PSD. We assume $\chi_1 = 0.3, \chi_2 = 0.2$. All the sources are considered to be at a fixed luminosity distance of 3 Gpc. To obtain the numerical estimates showed in this plot, we also consider a prior distribution on ϕ_c. To be precise, we assume ϕ_c to follow a Gaussian distribution with a zero mean and a variance of $1/\pi^2$.

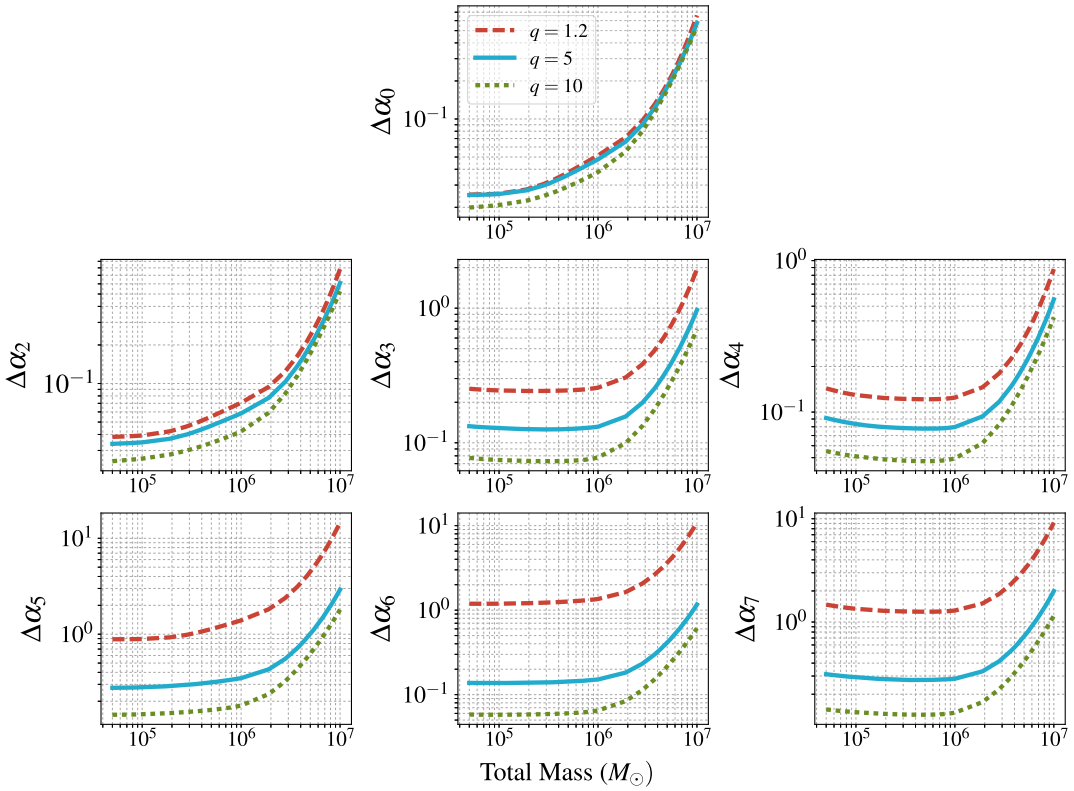

FIG. 5. Projected 1σ errors on the energy coefficients as a function of total mass for three different mass ratios $q = m_1/m_2 = 1.2, 5,$ and 10 in case of LISA noise PSD. We assume $\chi_1 = 0.9, \chi_2 = 0.8$. All the sources are considered to be at a fixed luminosity distance of 3 Gpc. To obtain the numerical estimates showed in this plot, we also consider a prior distribution on ϕ_c. To be precise, we assume the prior on ϕ_c to follow a Gaussian distribution with a zero mean and a variance of $1/\pi^2$.

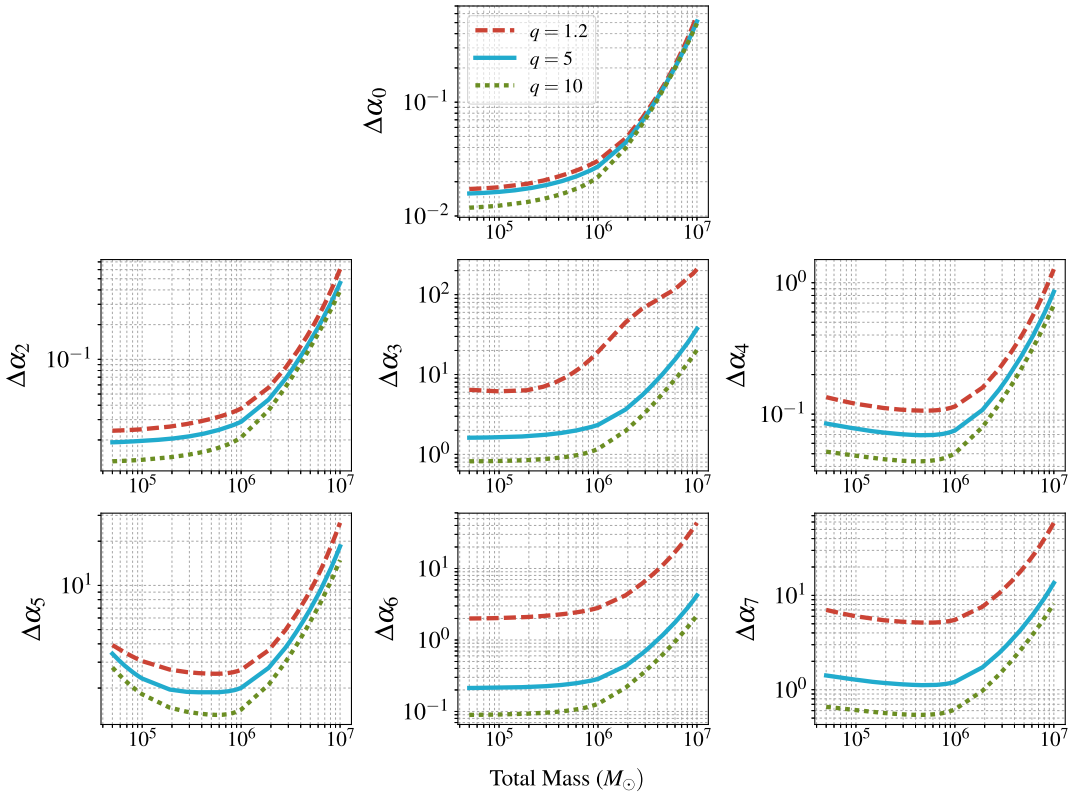

FIG. 6. Projected 1σ errors on the energy coefficients as a function of total mass for three different mass ratios $q = m_1/m_2 = 1.2, 5,$ and 10 in case of LISA noise PSD. We have considered $\chi_1 = 0.3, \chi_2 = 0.2$. All the sources are considered to be at a fixed luminosity distance of 3 Gpc. To obtain the numerical estimates showed in this plot, we also consider a prior distribution on ϕ_c. To be precise, we assume the prior on ϕ_c to follow a Gaussian distribution with a zero mean and a variance of $1/\pi^2$.

the same PN order with μ_2 (corresponding to the mass quadrupole) yielding the best constraint as it is the dominant multipole which contribute to the flux and the phasing. Due to the interplay between the sensitivity and mass dependent upper cutoff frequency, the errors increase as a function of mass in the regions of the parameter space we explore. The errors improve as the mass ratio increases for all cases except μ_2. As argued in Ref. [37], μ_2 is the only multipole parameter which appears both in the amplitude and the phase of the waveform and hence shows trends different from the other multipole coefficients. Inclusion of spins, on the whole, worsens the estimation of the multipole coefficients compared to the nonspinning case. This is expected as the spins increase the dimensionality of the parameter space but does not give rise to new features that helps the estimation. Effects such as spin-induced precession, which bring in a new time scale and associated modulations, may help counter this degradation in the parameter estimation. But this will be a topic for a future investigation. We also find that as a function of the spin magnitudes, the parameter estimation improves and hence highly spinning systems would yield stronger constraints on these coefficients. The estimation of various α_k, parametrizing the conservative dynamics, also broadly follow these trends. However, there is an important exception. The bounds on α_3 is consistently worse than those of α_4. This may be attributed to the important difference between them that α_3 parametrizes the 1.5PN term in the conserved energy which has only spin-dependent terms whereas the 2PN term contains both nonspinning and spinning contributions. Hence though α_4 is subleading in the PN counting, and hence the bounds are better.

We now discuss the quantitative results from these plots. One of the most interesting results is the projected constraints on coefficients that parametrize conservative dynamics. For third generation ground-based detectors, and for the prototypical source specifications, the bounds on 2PN conservative dynamics can be $\sim 10^{-2}$ which is comparable to or even better than the corresponding bounds expected from LISA. On the multipole coefficients side, the quadrupole coefficient μ_2 may be constrained to $\leq 10^{-1}(10^{-2})$ for second (third) generation detector network while the bounds from LISA are also $\sim 10^{-2}$. The best bounds for μ_3 are $\sim 10^{-1}, 10^{-2}, 10^{-2}$ for second generation, third generation and LISA, respectively, corresponding to highly spinning binaries. The projected bounds on the higher multipole coefficients from third generation detector network and LISA are comparable in all these cases, though one should keep in

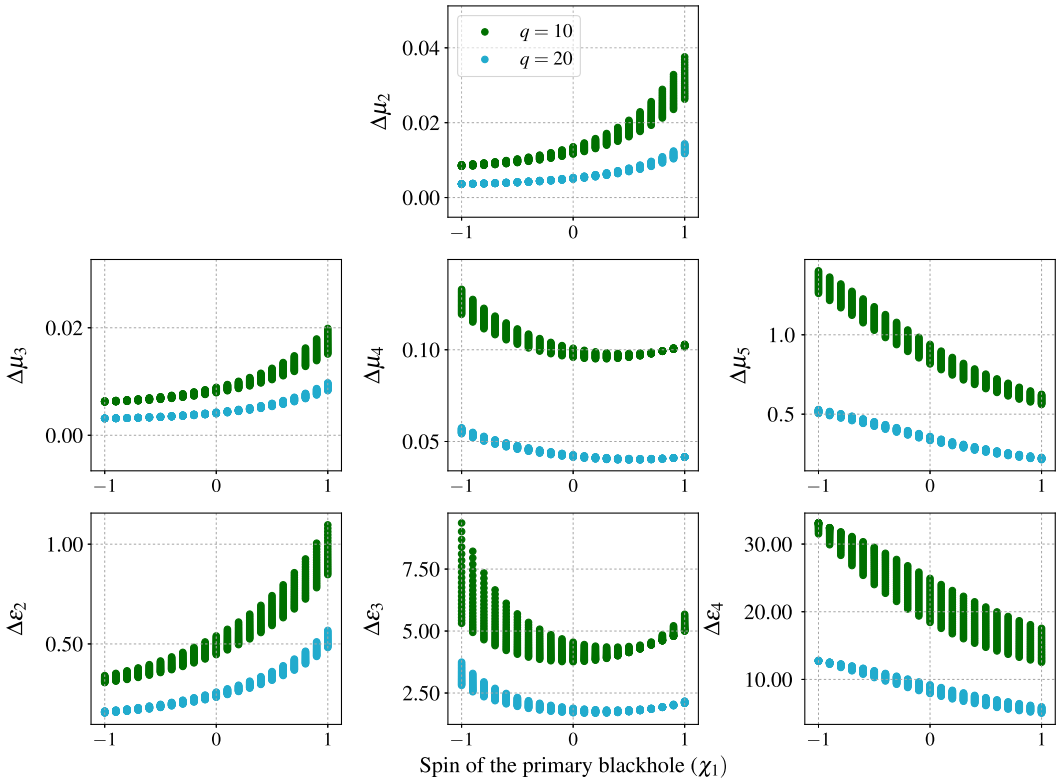

FIG. 7. Projected 1σ errors on multipole coefficients as a function of the spin of the heavier black hole, χ_1, for LISA noise PSD. All the sources are considered to be at a fixed luminosity distance of 3 Gpc with a total mass of 2×10^5 $M_\odot$. The green dots are for mass ratio 10 and the cyan dots denotes mass ratio 20. The vertical spread in the bounds at each χ_1 value is due to different χ_2 in the range $[-1, 1]$. To obtain the numerical estimates showed in this plot, we also consider a prior distribution on ϕ_c. To be precise, we assume the prior on ϕ_c to follow a Gaussian distribution with a zero mean and a variance of $1/\pi^2$.

mind the specifications of the sources we consider for these two cases are very different.

VII. CONCLUSION

We extend our previous work [37] by including spin effects in the inspiral dynamics and provide a waveform model, parametrized in terms of multipole and PN binding energy coefficients, for nonprecessing compact binaries in quasicircular orbit. The spin-orbit contributions are computed up to 3.5PN order while the spin-spin contributions are obtained up to 3PN order. We also provide the projected 1σ bounds on the multipole coefficients as well as the PN deviation parameters in the conserved energy for the second generation ground based detector network, the third generation ground based detector network and the space-based detector LISA, using the Fisher matrix approach. We find that the four leading order multipole coefficients and the four leading order PN conserved energy coefficients are measured with reasonable accuracy using these GW detectors.

We are currently in the process of implementing this parametrized waveform model presented in this paper in *LALInference* [109] to carry out tests of GR proposed here on real GW data. As a follow up, it will be interesting to compute the parametrized waveform within the effective-one-body formalism and investigate the possible bounds on these coefficients. Inclusion of higher modes of the gravitational waveforms, which contain these multipole coefficients in the amplitude of the waveform, will also be an interesting follow up in the future.

ACKNOWLEDGMENTS

S. K. and K. G. A. thank B. Iyer, G. Date, A. Ghosh, and J. Hoque for several useful discussions and N. V. Krishnendu for cross-checking some of the calculations reported here. We thank B. Iyer for critical reading of the manuscript and providing useful comments. K. G. A., A. G., S. K., and B. S. S. acknowledge the support by the Indo-US Science and Technology Forum through the Indo-US *Centre for the Exploration of Extreme Gravity*, Grant No. IUSSTF/JC-029/2016. A. G. and B. S. S. are supported in part by NSF Grants No. PHY-1836779, No. AST-1716394, and No. AST-1708146. K. G. A. is partially supported by a grant from Infosys Foundation, the Grant No. EMR/2016/005594 of SERB and Swarnajayanti Fellowship Grant No. DST/SJF/PSA-01/2017-18. C. V. D. B.

is supported by the research programme of the Netherlands Organisation for Scientific Research (NWO). Computing resources for this project were provided by the Pennsylvania State University. This document has LIGO preprint number LIGO-P1900136.

APPENDIX: SYSTEMATIC BIAS DUE TO THE USE OF NONSPINNING WAVEFORM MODEL FOR GW DETECTIONS BY PLANNED SPACE-BASED DETECTOR LISA

The use of inaccurate waveform model may lead to systematic biases in the parameter estimation [110,111]. For a detector data stream, s, consisting of a true waveform $\tilde{h}_{\rm T}(f;\vec{\theta}^{\rm T})$ and recovered with an approximate waveform $\tilde{h}_{\rm AP}(f;\vec{\theta}^{\rm best\ fit})$, the systematic errors on various parameters can be obtained by minimizing $\langle[\tilde{h}_{\rm T}(f;\vec{\theta}^{\rm T}) - \tilde{h}_{\rm AP}(f;\vec{\theta}^{\rm best\ fit})],[\tilde{h}_{\rm T}(f;\vec{\theta}^{\rm T}) - \tilde{h}_{\rm AP}(f;\vec{\theta}^{\rm best\ fit})]\rangle$ [110]. Since we are interested in quantifying the systematics due to the difference between the spinning and nonspinning waveforms, we adopt the minimization scheme developed in Ref. [110]. The basic assumption behind this scheme is to define a one parameter family of waveform models $(\tilde{h}^{\lambda}(f;\theta))$ that interpolate between both $\tilde{h}_{\rm T}(f;\vec{\theta}^{\rm T}) \equiv \tilde{h}^{\lambda=1}(f;\theta)$ and $\tilde{h}_{\rm AP}(f;\vec{\theta}) \equiv \tilde{h}^{\lambda=0}(f;\theta)$. As it turns out, after a set of approximations, the linearized estimate for the systematic error is (see Eq. (29) in Ref. [110])

$$\Delta_{\rm sys}\theta_m = (\Gamma^{-1}_{\rm AP})_{mk}\left\langle i\mathcal{A}\mu_2 f^{-7/6}\Delta\psi e^{i\psi}\Big|_{\theta=\theta^{\rm best\ fit}}, \frac{\partial\tilde{h}_{\rm AP}(f;\vec{\theta}^{\rm best\ fit})}{\partial\theta_k}\right\rangle, \tag{A1}$$

where $(\Gamma_{\rm AP})_{mk}$ is the Fisher matrix obtained from the approximate waveform $\tilde{h}_{\rm AP}(f;\vec{\theta})$ and $\Delta\psi = \psi_T - \psi_{\rm AP}$. All the quantities are evaluated at the best fit values of the parameters which coincide with the true values in the large SNR limit.

To quantify the systematic bias, we consider a six dimensional parameter space consists of $\{t_c, \phi_c, \ln\mathcal{A}, \ln\mathcal{M}_c, \ln\nu, \mu_\ell \text{ or } \epsilon_\ell\}$ to completely specify the approximate waveform $\tilde{h}_{\rm AP}(f;\vec{\theta}^{\rm best\ fit})$, for our purpose the parametrized nonspinning TaylorF2 waveform. We use the same approximate waveform to estimate the six dimensional Fisher matrix, $\Gamma_{\rm AP}$. On the other hand, we consider the parametrized nonprecessing TaylorF2 waveform to be our true waveform model.

In Fig. 8 we show the systematic biases on μ_2 and μ_3 for binaries with three different total masses, $M = 10^5$ $\mathrm{M}_\odot$, 10^6 $\mathrm{M}_\odot$, 10^7 $\mathrm{M}_\odot$ and mass ratio $q = 10$ as a function of individual spin parameter $\chi_1 = \chi_2 = \chi$ for LISA. Due to a smaller total mass ($M = 10^5$ $\mathrm{M}_\odot$) a large number of inspiral cycles reside in the LISA band. Hence even with very small spin values $\chi \sim \mathcal{O}(10^{-3})$, the systematic errors become larger than the statistical errors, which demands a parametrized spinning waveform model. In contrast, for larger total masses of about 10^6 $\mathrm{M}_\odot$ or 10^7 $\mathrm{M}_\odot$, the systematics affect the parameter estimation when the spin magnitude is slightly larger $\sim\mathcal{O}(10^{-1})$, as expected. Hence it is very crucial to incorporate the spin corrections in the waveform to reduce the effects of systematics when extracting the information about the multipole coefficients. We also find that as the total mass of binary increases the slope of the systematic bias curves changes from positive to negative for μ_2 and vice-versa for μ_3. This could be due to the nature of the correlation (positive or negative) between these multipole coefficients and the binary parameters (such as masses and spins) with increasing total mass. We quote the leading order estimates for the systematic biases in case of LISA only. Since the Fisher matrix-based leading order

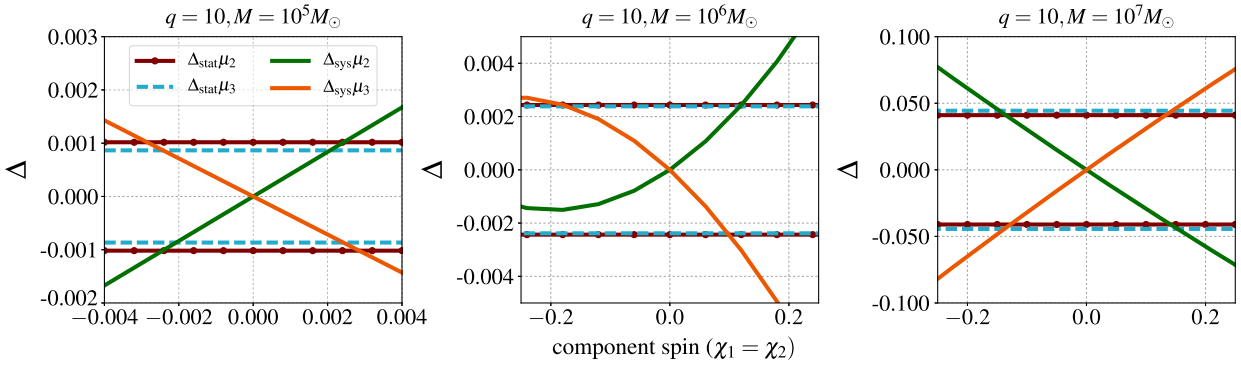

FIG. 8. Numerical estimates of systematic biases on the two leading multipole coefficients μ_2 and μ_3 as a function of $\chi_1 = \chi_2 = \chi$ for LISA noise PSD. We consider systems with three different total masses, $m = 10^5, 10^6, 10^7$ $M_\odot$ having mass ratio $q = 10$. All the sources are considered to be at a fixed luminosity distance of 3 Gpc.

estimation of systematic biases for network configuration demands reformulation of the prescription, we postpone these for future study in a more rigorous and accurate Bayesian framework.

We give the inputs needed to compute the phasing for TaylorT2, TaylorT3 and TaylorT4 in a Mathematica file (supl-Multipole-spin.m) which serves the Supplemental Material [112] to this paper.

[1] C. M. Will, Living Rev. Relativity **9**, 3 (2006).
[2] B. Sathyaprakash and B. Schutz, Living Rev. Relativity **12**, 2 (2009).
[3] N. Yunes and X. Siemens, Living Rev. Relativity **16**, 9 (2013).
[4] J. R. Gair, M. Vallisneri, S. L. Larson, and J. G. Baker, Living Rev. Relativity **16**, 7 (2013).
[5] E. Berti, E. Barausse, V. Cardoso, L. Gualtieri, P. Pani, U. Sperhake, L. C. Stein, N. Wex, K. Yagi, T. Baker *et al.*, Classical Quantum Gravity **32**, 243001 (2015).
[6] B. P. Abbott *et al.* (Virgo and LIGO Scientific Collaborations), Phys. Rev. Lett. **116**, 061102 (2016).
[7] B. P. Abbott *et al.* (Virgo and LIGO Scientific Collaborations), Phys. Rev. Lett. **116**, 241103 (2016).
[8] B. P. Abbott *et al.*, Phys. Rev. Lett. **118**, 221101 (2017).
[9] B. P. Abbott *et al.* (Virgo and LIGO Scientific Collaborations), Phys. Rev. X **6**, 041015 (2016).
[10] B. P. Abbott *et al.* (Virgo and LIGO Scientific Collaborations), Astrophys. J. **851**, L35 (2017).
[11] B. P. Abbott *et al.* (Virgo and LIGO Scientific Collaborations), Phys. Rev. Lett. **119**, 141101 (2017).
[12] B. P. Abbott *et al.* (LIGO Scientific and Virgo Collaborations), arXiv:1811.12907.
[13] J. Aasi *et al.* (LIGO Scientific Collaboration), Classical Quantum Gravity **32**, 115012 (2015).
[14] F. Acernese *et al.* (Virgo Collaboration), Classical Quantum Gravity **32**, 024001 (2015).
[15] B. P. Abbott *et al.* (Virgo and LIGO Scientific Collaborations), Phys. Rev. Lett. **116**, 221101 (2016).
[16] N. Yunes, K. Yagi, and F. Pretorius, Phys. Rev. D **94**, 084002 (2016).
[17] B. P. Abbott *et al.* (Virgo, Fermi-GBM, INTEGRAL, and LIGO Scientific Collaborations), Astrophys. J. **848**, L13 (2017).
[18] B. P. Abbott *et al.* (LIGO Scientific and Virgo Collaborations), arXiv:1811.00364.
[19] http://www.et-gw.eu/.
[20] S. Dwyer, D. Sigg, S. W. Ballmer, L. Barsotti, N. Mavalvala, and M. Evans, Phys. Rev. D **91**, 082001 (2015).
[21] M. Armano *et al.*, Phys. Rev. Lett. **116**, 231101 (2016).
[22] P. Amaro-Seoane, H. Audley, S. Babak, J. Baker, E. Barausse, P. Bender, E. Berti, P. Binetruy, M. Born, D. Bortoluzzi *et al.*, arXiv:1702.00786.
[23] K. G. Arun, B. R. Iyer, M. S. S. Qusailah, and B. S. Sathyaprakash, Classical Quantum Gravity **23**, L37 (2006).
[24] K. G. Arun, B. R. Iyer, M. S. S. Qusailah, and B. S. Sathyaprakash, Phys. Rev. D **74**, 024006 (2006).
[25] K. G. Arun, Classical Quantum Gravity **29**, 075011 (2012).
[26] N. Yunes and F. Pretorius, Phys. Rev. D **80**, 122003 (2009).
[27] C. K. Mishra, K. G. Arun, B. R. Iyer, and B. S. Sathyaprakash, Phys. Rev. D **82**, 064010 (2010).
[28] M. Agathos, W. Del Pozzo, T. G. F. Li, C. V. D. Broeck, J. Veitch, and S. Vitale, Phys. Rev. D **89**, 082001 (2014).
[29] T. G. F. Li, W. Del Pozzo, S. Vitale, C. Van Den Broeck, M. Agathos, J. Veitch, K. Grover, T. Sidery, R. Sturani, and A. Vecchio, Phys. Rev. D **85**, 082003 (2012).
[30] J. Meidam *et al.*, Phys. Rev. D **97**, 044033 (2018).
[31] N. Cornish, L. Sampson, N. Yunes, and F. Pretorius, Phys. Rev. D **84**, 062003 (2011).
[32] A. Ghosh *et al.*, Phys. Rev. D **94**, 021101 (2016).
[33] C. M. Will, Phys. Rev. D **50**, 6058 (1994).
[34] A. Królak, K. Kokkotas, and G. Schäfer, Phys. Rev. D **52**, 2089 (1995).
[35] C. M. Will, Phys. Rev. D **57**, 2061 (1998).
[36] S. Mirshekari, N. Yunes, and C. M. Will, Phys. Rev. D **85**, 024041 (2012).
[37] S. Kastha, A. Gupta, K. G. Arun, B. S. Sathyaprakash, and C. Van Den Broeck, Phys. Rev. D **98**, 124033 (2018).
[38] K. Thorne, Rev. Mod. Phys. **52**, 299 (1980).
[39] L. Blanchet, T. Damour, and B. R. Iyer, Phys. Rev. D **51**, 5360 (1995).
[40] L. Blanchet, T. Damour, B. R. Iyer, C. M. Will, and A. G. Wiseman, Phys. Rev. Lett. **74**, 3515 (1995).
[41] L. Blanchet, B. R. Iyer, C. M. Will, and A. G. Wiseman, Classical Quantum Gravity **13**, 575 (1996).
[42] L. Blanchet, B. R. Iyer, and B. Joguet, Phys. Rev. D **65**, 064005 (2002); **71**, 129903(E) (2005).
[43] L. Blanchet, T. Damour, G. Esposito-Farèse, and B. R. Iyer, Phys. Rev. Lett. **93**, 091101 (2004).
[44] M. A. Abramowicz and W. Kluzniak, Astron. Astrophys. **374**, L19 (2001).
[45] L. Gou, J. E. McClintock, R. A. Remillard, J. F. Steiner, M. J. Reid, J. A. Orosz, R. Narayan, M. Hanke, and J. García, Astrophys. J. **790**, 29 (2014).
[46] C. S. Reynolds, Classical Quantum Gravity **30**, 244004 (2013).
[47] L. Kidder, C. Will, and A. Wiseman, Phys. Rev. D **47**, R4183 (1993).
[48] T. A. Apostolatos, Phys. Rev. D **52**, 605 (1995).
[49] L. Kidder, Phys. Rev. D **52**, 821 (1995).
[50] E. Poisson, Phys. Rev. D **57**, 5287 (1998).
[51] B. Mikóczi, M. Vasúth, and L. A. Gergely, Phys. Rev. D **71**, 124043 (2005).

[52] L. Blanchet, A. Buonanno, and G. Faye, Phys. Rev. D **74**, 104034 (2006); **75**, 049903(E) (2007).
[53] K. G. Arun, A. Buonanno, G. Faye, and E. Ochsner, Phys. Rev. D **79**, 104023 (2009).
[54] L. Blanchet, A. Buonanno, and G. Faye, Phys. Rev. D **84**, 064041 (2011).
[55] A. Bohe, S. Marsat, G. Faye, and L. Blanchet, Classical Quantum Gravity **30**, 075017 (2013).
[56] A. Bohé, S. Marsat, and L. Blanchet, Classical Quantum Gravity **30**, 135009 (2013).
[57] A. Bohé, G. Faye, S. Marsat, and E. K. Porter, Classical Quantum Gravity **32**, 195010 (2015).
[58] L. Blanchet, Living Rev. Relativity **17**, 2 (2014).
[59] J. Hartung and J. Steinhoff, Ann. Phys. (Berlin) **523**, 783 (2011).
[60] M. Levi, Phys. Rev. D **85**, 064043 (2012).
[61] S. Marsat, A. Bohe, G. Faye, and L. Blanchet, Classical Quantum Gravity **30**, 055007 (2013).
[62] M. Levi and J. Steinhoff, J. Cosmol. Astropart. Phys. 01 (2016) 011.
[63] S. Marsat, A. Bohè, L. Blanchet, and A. Buonanno, Classical Quantum Gravity **31**, 025023 (2014).
[64] S. Marsat, Classical Quantum Gravity **32**, 085008 (2015).
[65] A. Buonanno, G. Faye, and T. Hinderer, Phys. Rev. D **87**, 044009 (2013).
[66] C. Will and A. Wiseman, Phys. Rev. D **54**, 4813 (1996).
[67] J. Hartung and J. Steinhoff, Ann. Phys (Berlin) **523**, 919 (2011).
[68] M. Levi, Phys. Rev. D **82**, 064029 (2010).
[69] M. Levi and J. Steinhoff, J. Cosmol. Astropart. Phys. 12 (2014) 003.
[70] M. Levi and J. Steinhoff, J. High Energy Phys. 06 (2015) 059.
[71] M. Levi and J. Steinhoff, J. Cosmol. Astropart. Phys. 01 (2016) 008.
[72] M. Levi and J. Steinhoff, J. High Energy Phys. 09 (2015) 219.
[73] M. Levi and J. Steinhoff, arXiv:1607.04252.
[74] L. Blanchet and T. Damour, Phil. Trans. R. Soc. A **320**, 379 (1986).
[75] L. Blanchet and T. Damour, Phys. Rev. D **37**, 1410 (1988).
[76] L. Blanchet and G. Schäfer, Mon. Not. R. Astron. Soc. **239**, 845 (1989).
[77] L. Blanchet, Phys. Rev. D **51**, 2559 (1995).
[78] T. Damour, P. Jaranowski, and G. Schäfer, Phys. Rev. D **63**, 044021 (2001); **66**, 029901(E) (2002).
[79] L. Blanchet, Living Rev. Relativity **9**, 4 (2006).
[80] E. Racine, A. Buonanno, and L. E. Kidder, Phys. Rev. D **80**, 044010 (2009).
[81] T. Damour, P. Jaranowski, and G. Schäfer, Phys. Lett. B **513**, 147 (2001).
[82] L. Blanchet, T. Damour, and G. Esposito-Farèse, Phys. Rev. D **69**, 124007 (2004).
[83] V. de Andrade, L. Blanchet, and G. Faye, Classical Quantum Gravity **18**, 753 (2001).
[84] L. Blanchet and B. R. Iyer, Classical Quantum Gravity **20**, 755 (2003).
[85] Y. Itoh and T. Futamase, Phys. Rev. D **68**, 121501(R) (2003).
[86] L. Blanchet, G. Faye, B. R. Iyer, and B. Joguet, Phys. Rev. D **65**, 061501(R) (2002); **71**, 129902(E) (2005).
[87] B. S. Sathyaprakash and S. V. Dhurandhar, Phys. Rev. D **44**, 3819 (1991).
[88] T. Damour, B. R. Iyer, and B. S. Sathyaprakash, Phys. Rev. D **62**, 084036 (2000).
[89] A. Buonanno, B. Iyer, E. Ochsner, Y. Pan, and B. S. Sathyaprakash, Phys. Rev. D **80**, 084043 (2009).
[90] C. Cutler, Phys. Rev. D **57**, 7089 (1998).
[91] C. K. Mishra, A. Kela, K. G. Arun, and G. Faye, Phys. Rev. D **93**, 084054 (2016).
[92] M. Wade, J. D. E. Creighton, E. Ochsner, and A. B. Nielsen, Phys. Rev. D **88**, 083002 (2013).
[93] N. V. Krishnendu, K. G. Arun, and C. K. Mishra, Phys. Rev. Lett. **119**, 091101 (2017).
[94] N. V. Krishnendu, C. K. Mishra, and K. G. Arun, Phys. Rev. D **99**, 064008 (2019).
[95] C. Rao, Bull. Calcutta Math. Soc. **37**, 81 (1945).
[96] H. Cramer, *Mathematical Methods in Statistics* (Pergamon Press, Princeton University Press, Princeton, NJ, 1946).
[97] C. Cutler and E. Flanagan, Phys. Rev. D **49**, 2658 (1994).
[98] K. G. Arun, B. R. Iyer, B. S. Sathyaprakash, and P. A. Sundararajan, Phys. Rev. D **71**, 084008 (2005); **72**, 069903 (E) (2005).
[99] M. Vallisneri, Phys. Rev. D **77**, 042001 (2008).
[100] Y. Aso, Y. Michimura, K. Somiya, M. Ando, O. Miyakawa, T. Sekiguchi, D. Tatsumi, and H. Yamamoto (KAGRA Collaboration), Phys. Rev. D **88**, 043007 (2013).
[101] B. Iyer *et al.*, LIGO-India Technical Report No. LIGO-M1100296, 2011.
[102] P. Ajith, Phys. Rev. D **84**, 084037 (2011).
[103] https://dcc.ligo.org/LIGO-T1500293/public.
[104] https://git.ligo.org/lscsoft/lalsuite/blob/master/lal/python/lal/antenna.py.
[105] B. P. Abbott *et al.* (LIGO Scientific Collaboration), Classical Quantum Gravity **34**, 044001 (2017).
[106] B. Abbott, R. Abbott, T. Abbott, M. Abernathy, K. Ackley, C. Adams, P. Addesso, R. Adhikari, V. Adya, C. Affeldt *et al.*, Classical Quantum Gravity **34** (2017).
[107] S. Babak, J. Gair, A. Sesana, E. Barausse, C. F. Sopuerta, C. P. L. Berry, E. Berti, P. Amaro-Seoane, A. Petiteau, and A. Klein, arXiv:1703.09722.
[108] E. Berti, A. Buonanno, and C. M. Will, Phys. Rev. D **71**, 084025 (2005).
[109] J. Veitch *et al.*, Phys. Rev. D **91**, 042003 (2015).
[110] C. Cutler and M. Vallisneri, Phys. Rev. D **76**, 104018 (2007).
[111] M. Favata, Phys. Rev. Lett. **112**, 101101 (2014).
[112] Please see the Supplemental Material at http://link.aps.org/supplemental/10.1103/PhysRevD.100.044007 for the inputs to compute the phasing for TaylorT2, TaylorT3 and TaylorT4 approximants.